

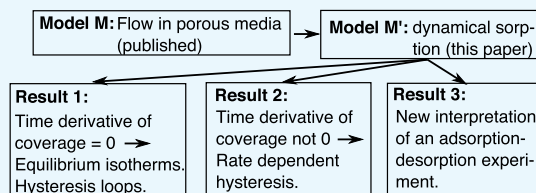
1 Dynamics of Monolayer Physisorption in Homogeneous 2 Mesoporous Media

3 Paul Papatzacos*¹

4 Department of Mathematics and Physics, University of Stavanger, 4036 Stavanger, Norway

5 **ABSTRACT:** A model for monolayer physisorption of a one-
6 component gas on the pore surface of a homogeneous macroporous
7 or mesoporous porous medium is presented. It originates from an
8 averaging over many pores of a macroporous medium filled with a one-
9 component fluid. The resulting model does not assume anything about
10 pore shape, but assumes that the pores are so large that capillary
11 condensation does not occur. Mathematically, the model gives coverage

12 as the solution of an ordinary, first-order, differential equation, where the
13 time derivative of coverage is proportional to the difference between the chemical potential of the adsorbate and the chemical
14 potential of the ambient gas. Coverage is determined by the ambient gas density, with temperature, adsorbate critical
15 temperature, and the Henry adsorption constant as parameters. The rest of this abstract describes what is deduced from the
16 equations of the model. Adsorbate phase transitions are built into the model by the use of van der Waals equations of state.
17 Equilibrium isotherms are derived from the equality of the chemical potentials. The differential equation for coverage makes it
18 possible to determine the mathematical stability of the equilibrium isotherms, and a number of properties of the isotherms are
19 derived, the most important being as follows: (i) an adsorbate phase transition is always accompanied by a well-defined
20 hysteresis loop, although “loop” is somewhat misleading as its vertical boundaries do not consist of equilibrium states; (ii) the
21 vertical boundaries are exactly located; (iii) the upper and lower boundaries consist of states that are mathematically stable,
22 while being either physically stable or metastable, and if physical metastability is the case, then the actual state of the adsorbate
23 (mono- or bi-phasic) will not be visible on the equilibrium isotherm. The shapes of the equilibrium isotherms are largely
24 determined by the value of the Henry constant, whether the isotherms are subcritical or supercritical. Expressions for the
25 location of an equilibrium isotherm’s region of fastest variation and for the locations of the vertical boundaries of its hysteresis
26 loop are found that also show the importance of Henry’s constant. Dynamical, that is, time-dependent isotherms are presented
27 for the case describing the variation of coverage resulting from forcing the ambient gas to undergo a compression–
28 decompression loop. Two subcases are considered: the subcritical and the supercritical adsorbate. It is shown that coverage in
29 terms of ambient pressure exhibits closed loops, even in supercritical isotherms. However, supercritical loops shrink when the
30 cycle time increases, reminiscent of rate-dependent hysteresis observed in piezoelectricity. The model is used to interpret two
31 experiments on the sorption of CO₂ and CH₄ on coal that showed hysteresis loops in isotherms of supercritical adsorbates and
32 that were originally interpreted as leading to different Henry constants for adsorption and for desorption. The interpretation set
33 forth here uses the inherent dynamics of the model and looks at the loop as just one isotherm evolving in time, thus leading to a
34 unique Henry constant.



1. INTRODUCTION

35 In experiments on gas physisorption, one often observes a
36 discontinuity in the equilibrium isotherms and a hysteresis
37 loop. See Morishige and Shikimi¹ and references given there.
38 The step and the loop occur at temperatures well below the
39 critical temperature of the ambient gas, and at pressures well
40 below its saturation pressure.

41 It has been shown by Hill, in an article published in 1947,²
42 that hysteresis can be explained by assuming the existence of
43 metastable adsorbed states in monolayer physisorption, no
44 assumptions about the pores being necessary. Hill’s result is
45 generalized in the present article, where monolayer phys-
46 isorption is used to the exclusion of other processes. It must be
47 mentioned that monolayer physisorption in a mesoporous or
48 macroporous medium is, in a certain sense, in a class by itself,
49 possibly together with multilayer physisorption if the number
50 of layers is on the order of two or three. It has indeed been

shown³ that the size of the pore surface per unit volume of a
51 mesoporous or macroporous medium is such that the amount
52 adsorbed by monolayer physisorption is negligibly small when
53 compared to the amount that flows in the pores. On the other
54 hand, physisorption by capillary condensation and/or chem-
55 isorption deal with adsorbed amounts that differ by orders of
56 magnitude from those occurring in monolayer physisorption
57 and are essential to describe such processes as industrial
58 hydrocarbon recovery. Capillary condensation and chemisorp-
59 tion are not considered in any detail in this article. 60

The generalization of Hill’s result is done in the framework
61 of a sorption model, called M’ for convenience here. M’, a
62 special case of a model M to be described presently, expresses 63

Received: September 11, 2019

Accepted: November 27, 2019

64 the rate of change of coverage in terms of the coverage itself, of
65 the ambient gas density, of temperature, of the critical
66 temperatures of adsorbate and ambient gas, and of Henry's
67 adsorption constant. This is not the first appearance of an
68 equation for the rate of change of coverage (see Alfé and
69 Gillan⁴), but it is, to the author's knowledge, the first time such
70 an equation leads to an understanding of hysteresis loops in
71 adsorption, and to a reinterpretation of experimental results.
72 The three paragraphs below are short presentations of results
73 that are described in more detail in Sections 2, 3, and 4.

74 The first result concerns the placement of the vertical
75 boundaries of the hysteresis loop (Section 2.5). Ball and
76 Evans,⁵ in their article on the mechanism for hysteresis, noted
77 that the existence of physically metastable states will bring
78 about a transition to a physically stable state at some ambient
79 pressure and thus produce a vertical boundary for the
80 hysteresis loop at that pressure in adsorption as well as in
81 desorption. They also remarked that determining the transition
82 pressure is beyond the scope of an equilibrium theory, given
83 that there are infinitely many physically metastable states. Now
84 M' describes the evolution of isotherms with time, and it also
85 determines the equilibrium isotherms. This implies that the
86 mathematical stability of any point on an equilibrium isotherm
87 can be found, and it turns out that physically metastable states
88 are mathematically stable, except for just two such points, one
89 for adsorption and one for desorption: these are mathemati-
90 cally unstable and determine the transition pressures.

91 The second result concerns the new possibility implied by
92 the ability of M' to describe time-dependent isotherms. This
93 has a direct relevance to measurements where adsorption and
94 desorption follow different paths that join at a low and a high
95 coverage, thus exhibiting a loop^{7,6} with no vertical boundaries.
96 The explanation given by M' is the one given by other
97 workers: a genuine hysteresis loop must have two vertical
98 boundaries, so their absence is explained by appealing to an
99 insufficient equilibration time⁶ or waiting time.⁸ There is,
100 however, a new possibility implied by the ability of M' to
101 describe time-dependent isotherms: that of considering the
102 noncoinciding adsorption and desorption paths as being just
103 one isotherm evolving in time under the application of a
104 pressure-cycle consisting of compression followed by decom-
105 pression of the ambient gas. The isotherms resulting from such
106 a cycle are shown in Section 3, for the two cases of a
107 supercritical and a subcritical isotherm.

108 The third result concerns the interpretation of experiments
109 on sorption of methane (important as a source of energy) and
110 on sorption of carbon dioxide (an important product to
111 sequester). These two cases of sorption are exceptional in
112 that they cannot be described in the framework of capillary
113 condensation: the critical temperatures of the substances are
114 low compared to storage temperatures, so that capillary
115 condensation cannot occur. Wang et al.⁹ enumerate, and give
116 references for, the hypotheses that have been made to explain
117 the mechanism of methane and carbon dioxide sorption
118 hysteresis: residual moisture in coal samples, surface geometry
119 heterogeneity, chemical interaction, structural deformation,
120 experimental inaccuracies, and insufficient waiting time. They
121 conclude that the mechanism remains an open question. The
122 most straightforward way to describe CH_4 and CO_2 sorption
123 has been to use the Langmuir model: see Jessen et al.⁷ See also
124 Wang et al.⁹ who look at two additional isotherms, one from
125 the Dubinin–Radushkevich model and one from the dual
126 sorption model, the latter allowing the inclusion of the effect of

coal swelling. Section 4 of the present article gives an
127 alternative description, based on the second result above,
128 that leads to a unique value for the Henry constant instead of
129 the two obtained by fitting separate equilibrium isotherms, one
130 for adsorption and another for desorption.⁷

131 It is also worth mentioning that the mathematical expression
132 of M' is simple enough to allow approximate expressions for a
133 number of useful quantities, such as the pressure at which the
134 isotherm is steepest and the width of the hysteresis loop.

135 A short description of model M' and of the underlying
136 model M , follows.

137 M is a model for multiphase flow in a porous medium, based
138 on the diffuse interface assumption.¹⁰ It is the result of an
139 averaging over many pores of the equations describing
140 Navier–Stokes flow in the pores. The averaging leads to a
141 new set of equations involving averaged quantities such as
142 density, velocity components, temperature, internal energy,
143 and entropy. M , and thereby M' , are based on the following
144 assumptions: (a1) the fluid-containing pores are connected;
145 (a2) the smallest pore-throat diameter is large when compared
146 to the average distance between fluid molecules, and also when
147 compared to their mean free path; (a3) adsorption occurs by
148 physisorption; (a4) adsorption is monolayer; (a5) the heat
149 generally released by adsorption does not appreciably change
150 the temperature; (a6) the averaged fluid quantities obey the
151 same thermodynamical laws as the quantities of the original
152 fluid and, in particular, the averaged fluid has a well-defined
153 pressure obeying an equation of state that can be chosen
154 among the known ones.

155 M' contains three additional assumptions: (a7) the averaged
156 adsorbed fluid is assumed to have the thermodynamics of a
157 two-dimensional fluid with, in particular, a spreading pressure
158 (the negative of the surface tension)¹¹ obeying a van der Waals
159 equation of state; (a8) the ambient fluid is monophasic; (a9)
160 any externally applied changes, such as compressions or
161 decompressions, are done so slowly that the ambient fluid
162 velocity is negligibly small.

163 The consequences of these assumptions are discussed
164 presently, after the introduction of the basic equations of M' .
165 These are obtained directly from M (see eq 17 in
166 Papatzacos¹⁰), with a slight modification in notation

$$\dot{c}_\Sigma = -\Delta\mu \quad (1)$$

$$\Delta\mu = L(\mu_\Sigma - \mu_f) \quad (2)$$

167 The dot in the first equation denotes partial differentiation
168 with respect to time. A space dependence can also be included
169 for c_Σ , but is ignored here, as it is shown below that the
170 assumptions of model M' make it redundant. At the level of
171 model M , μ_f is the chemical potential of the ambient fluid,
172 modified by the addition of two terms: a term proportional to
173 the Laplacian of the ambient fluid density and a term
174 proportional to the squared modulus of the ambient fluid
175 velocity. The Laplacian originates in the diffuse interface
176 framework, where large gradients of density exist in the
177 interfaces between phases, if two phases coexist. The squared
178 velocity accounts for the kinetic energy exchanged between
179 ambient and adsorbed fluids. The two equations above are the
180 core of model M' . They lead, after some preliminaries
181 presented as background material in Section 5, to a differential
182 equation for the coverage, presented in Section 5.4.

183 The consequences of assumptions (a1) to (a9) are as
184 follows.

188 As a result of the averaging process, the individual
189 characteristics of the pores are lost, leaving only two
190 parameters to characterize the medium as a whole, which are
191 porosity and pore surface per unit volume.¹⁰

192 Assumptions (a1), (a2), and (a4) imply that adsorption
193 does not affect the basic description of the ambient fluid by the
194 equations of fluid mechanics expressing balance of mass,
195 momentum, energy, and entropy. They also imply that
196 adsorption induces negligible changes in the values of porosity
197 and pore surface per unit volume. In fact, assumption (a4)
198 implies, as stated above, that inside an arbitrary volume of
199 porous medium, the total mass adsorbed is negligibly small
200 when compared to the mass of fluid that can flow freely in the
201 pores.³ Assumption (a5) implies that the quantities character-
202 izing the ambient fluid, such as its density and temperature and
203 consequently its pressure and chemical potential, are not
204 modified by sorption. (On the other hand, the quantities
205 characterizing the adsorbed fluid are determined by the
206 ambient fluid.) Assumption (a7) implies that phase transitions
207 can occur in the adsorbate. Assumption (a8) implies that no
208 interfaces exist in the ambient fluid, so that the Laplacian of the
209 ambient density that modifies the chemical potential is
210 negligible. Assumption (a9) implies that the other term
211 modifying the chemical potential of the ambient fluid is
212 negligibly small. With these last two assumptions, μ_f is the
213 usual chemical potential of the ambient fluid. Another
214 consequence of (a8) and (a9) is that eqs 1 and 2 are space
215 independent.

216 It is here emphasized that, as already mentioned, isotherm
217 properties deduced in M' , like adsorbate phase transitions or
218 hysteresis loops, do not depend on assumptions about the
219 shape of the pores and, in particular, occur without the
220 occurrence of capillary condensation.

221 The thermodynamical description of the fluids is given as
222 background material in Section 5, where explicit expressions
223 for the pressure, spreading pressure, and chemical potentials
224 are given, and where Henry's adsorption constant is
225 introduced. As already mentioned, the adsorbate is a van der
226 Waals fluid, whereas three alternatives are considered for the
227 ambient fluid: ideal with zero volume particles (called ideal
228 type 0), ideal with nonzero volume particles (called ideal type
229 1), and van der Waals. The $\Delta\mu$ of eqs 1 and 2 above is then
230 derived as a function of coverage, ambient density, and some
231 parameters that include temperature and Henry's constant.
232 The concepts of physical stability, metastability, and instability,
233 known to occur in connection with the van der Waals equation
234 of state, are illustrated in figures in the same section, for easy
235 reference in the rest of the article.

236 The derivation of the basic differential equation defining M'
237 is given as background material in Section 5.4. Other basic
238 properties of M' , specifically the definitions of equilibrium
239 isotherms and of mathematical stability are given in Section 2.

2. RESULT AND DISCUSSION 1: THEORY OF EQUILIBRIUM ISOTHERMS

241 Equilibrium isotherms are defined in Section 2.1. Mathematical
242 stability is defined in Section 2.2, and is followed by a section
243 on equilibrium isotherms given by analytical expressions, then
244 by two sections on equilibrium isotherms given by numerical
245 solutions.

246 **2.1. Definition of an Equilibrium Isotherm.** It is here
247 referred to Section 5.4, where the differential equation giving
248 the time rate of change of coverage is deduced, that is, eq 59.

The equilibrium isotherms follow from this equation: they are
the solutions that have zero rate of change. There are
additional requirements concerning stability and unicity: see
the last paragraph but one of this section.

An equilibrium solution is defined as follows. Given \tilde{T} , $\tilde{T}_{\Sigma c}$,
and ψ , an equilibrium solution of eq 59 is a set of points $(r_e,$
 $\theta_e)$ in a Cartesian plane, satisfying $0 < r_e \leq r_{gr}$, $0 < \theta_e < 1$, and

$$\Delta\tilde{\mu}(\theta_e, r_e, \tilde{T}, \tilde{T}_{\Sigma c}, \psi) = 0 \quad (3)$$

An equivalent form of eq 3 is found as follows. The equation
is first rewritten as $\tilde{\mu}_{\Sigma, \text{red}} - \tilde{T} \ln \tilde{K}_H = \tilde{\mu}_{f, \text{red}}$ by using eqs 56 and
57. Dividing both sides by \tilde{T} , exponentiating, and referring to
eq 45, one finds

$$\tilde{f}_{\Sigma}(\theta, \tilde{T}, \tau) = \tilde{K}_H \tilde{f}_f(r, \tilde{T}) \quad (4)$$

This equation, with another definition for the proportion-
ality constant, is identical with eq 4 in the article by Hoory and
Prausnitz.¹²

Equations 3 and/or 4 give equilibrium isotherms provided
that (i) points that represent mathematically and/or physically
unstable states are discarded, and that (ii) non-unicity of θ_e for
any r_e agrees with observations of hysteresis.

Physical stability is considered in Section 5.1; mathematical
stability is defined in Section 2.2.

2.2. Mathematical Stability of Equilibrium Isotherms.

Mathematical stability, or m -stability, of equilibrium isotherms,
is defined as follows.¹³

For any given set $\{r_e, \tilde{T}, \tilde{T}_{\Sigma c}, \psi\}$, a solution θ_e of eq 3 or 4 is
said to be (asymptotically) m -stable if there is a neighborhood
of θ_e such that any θ inside this neighborhood approaches θ_e as
time increases.

It follows from the definition that a very simple criterion for
deciding whether any point on an equilibrium isotherm is m -
stable is as follows:

θ_e is an m -stable equilibrium solution if and only if $\Delta\tilde{\mu}$
changes from negative to positive values when $\theta - \theta_e$ does so.

Indeed, referring to Figure 1, and keeping eq 59 in mind,
one sees that, if the condition is satisfied, then any perturbation

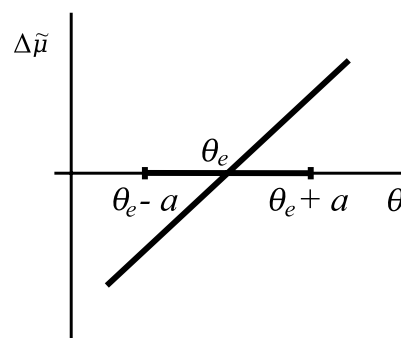


Figure 1. Figure used in defining m -stability in Section 2.2. If $\Delta\tilde{\mu}$ vs θ
behaves as shown in the vicinity of θ_e , then θ_e is m -stable.

of θ_e that takes place during time $d\tilde{t} > 0$, and that brings θ in
the interval $(\theta_e, \theta_e + a)$, gives rise to $\Delta\tilde{\mu} > 0$. It follows that $d\theta$
 $= -\Delta\tilde{\mu} d\tilde{t} < 0$, so that θ is drawn back to θ_e . A similar
reasoning can be made for a perturbation that brings θ to the
left of θ_e , with the same conclusion that θ is drawn back to θ_e .
Necessity is also easily proven.

2.3. Analytical Equilibrium Isotherms and Their Stability. Analytical solutions of eq 4 are considered here. 292

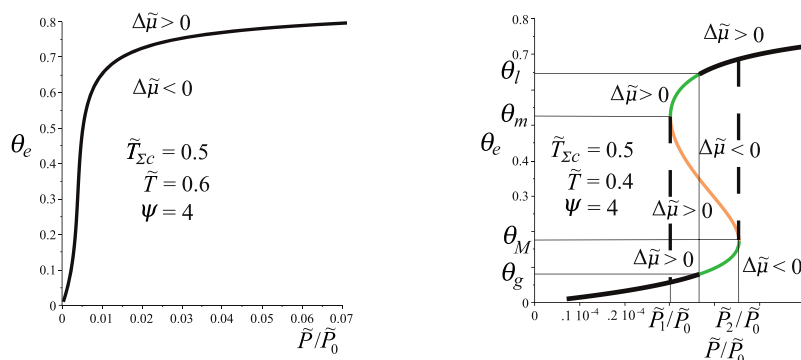


Figure 2. Plots of eq 6, for a supercritical (left) or subcritical (right) adsorbate for values of \tilde{T} , $\tilde{T}_{\Sigma c}$, and ψ , as indicated. The right plot uses the notations of Figure 14 for the subscripted θ 's, as well as for the meanings of the colors. Concerning the vertical dashed lines in the right plot, see Section 2.3.

293 More precisely, one seeks to express θ_e as a known function of
 294 r_e or vice versa. Obviously, this is only possible if one knows
 295 how to invert either \tilde{f}_{Σ} or \tilde{f}_f . No inverse of \tilde{f}_{Σ} , given by eq 46
 296 (right), is known. Inverting \tilde{f}_f however, may be possible as
 297 shown below. There are three acceptable approximations for the
 298 ambient fluid fugacity, and two of them are invertible: the
 299 ones obtained by assuming that the ambient fluid is ideal,
 300 either of type zero (zero volume particles) or of type 1
 301 (nonzero volume particles). The relevant expressions for \tilde{f}_f are
 302 given in eq 47 (right) and 48 (right). In fact, most analytical
 303 isotherms are expressions giving pressure as a function of
 304 coverage, see for example, Table I-1 in the book by Ross and
 305 Olivier.¹⁴ This can easily be done in the present case by writing
 306 each invertible fugacity in terms of the corresponding pressure.
 307 Referring to the left and center equations of the set (36), it is
 308 easily seen that

$$\tilde{f}_f^{\text{id0}} = \tilde{p}^{\text{id0}}, \quad \tilde{f}_f^{\text{id1}} = \tilde{p}^{\text{id1}} \exp\left(\frac{\tilde{p}^{\text{id1}}}{\tilde{T}}\right)$$

309 Assuming that the ambient gas can be approximated by an
 310 ideal gas of type 0, eq 4 gives the known expression

$$\tilde{p}^{\text{id0}} = \frac{\tilde{f}_{\Sigma}}{\tilde{K}_H} = \frac{\tilde{T}}{\tilde{K}_H} \frac{\theta_e}{1 - \theta_e} \exp\left(\frac{\theta_e}{1 - \theta_e} - \frac{27\theta_e}{\tau}\right) \quad (5)$$

312 Assuming that the ambient gas can be approximated by an
 313 ideal gas of type 1, eq 4 gives

$$\frac{\tilde{f}_{\Sigma}}{\tilde{K}_H \tilde{T}} = \frac{\tilde{p}^{\text{id1}}}{\tilde{T}} \exp\left(\frac{\tilde{p}^{\text{id1}}}{\tilde{T}}\right)$$

314 This equation is of the type $Z \exp Z = g$ and, g being
 315 positive, is equivalent to $Z = \text{Wp}(g)$, where Wp is the principal
 316 part of the Lambert W -function.¹⁵ One thus obtains

$$\begin{aligned} \tilde{p}^{\text{id1}} &= \tilde{T} \text{Wp}\left(\frac{\tilde{f}_{\Sigma}}{\tilde{K}_H \tilde{T}}\right), \\ &= \tilde{T} \text{Wp}\left(\frac{1}{\tilde{K}_H} \frac{\theta_e}{1 - \theta_e} \exp\left(\frac{\theta_e}{1 - \theta_e} - \frac{27\theta_e}{\tau}\right)\right) \end{aligned} \quad (6)$$

318 To the author's knowledge, this equation has not previously
 319 appeared in the adsorption literature. A plot of θ_e versus \tilde{p}^{id0} is
 320 usually quite close to a plot of θ_e versus \tilde{p}^{id1} , except for ψ -
 321 values less than 1 and for θ_e -values close to 1.

322 One now turns to the restrictions mentioned in Section 2.1,
 323 so as to establish whether the expressions above are acceptable.

324 Plots of eq 6, say, show continuous curves, monotonic
 325 increasing when $\tilde{T} > \tilde{T}_{\Sigma c}$ (Figure 2, left-hand plot), but with a
 326 region of three-valuedness when $\tilde{T} < \tilde{T}_{\Sigma c}$ (Figure 2, right
 327 plot).^a

328 The m-stability of the supercritical isotherm (left plot of
 329 Figure 2) is established as follows. Letting θ move on a vertical
 330 line, say upward from a low value, then $\theta - \theta_e$ and $\Delta\tilde{\mu}$ both go
 331 from negative to positive values when the isotherm is crossed.
 332 The necessary and sufficient condition stated in Section 2.2 is
 333 satisfied, so that the supercritical isotherm is m-stable. It is also
 334 physically stable (p-stable) because ambient gas and the
 335 adsorbate behave nearly ideally. One thus recovers the known
 336 result that the supercritical isotherms given by eq 5 are
 337 physically correct.

338 Turning to the subcritical case (right plot of Figure 2), one
 339 sees that the isotherm has three parts: a central part, whose
 340 states are p-unstable (orange line), connecting a lower to an
 341 upper part. The lower is here called the adsorption branch, and
 342 the upper is called the desorption branch. Each of these
 343 branches contains a set of p-stable states (black line) and a set
 344 of p-metastable states (green line). The m-stabilities of the
 345 three parts are established by the same argument as used in the
 346 supercritical case. One easily finds that the central part (orange
 347 line) consists of m-unstable states, so that there is no doubt in
 348 discarding these points that already are p-unstable. However,
 349 all points on the adsorption and desorption branches are, with
 350 the exception of one point for each branch, m-stable, regardless
 351 of the quality of their physical stability: the whole set of p-
 352 stable points and almost the whole set of p-metastable points
 353 are m-stable. The exception is, for each branch, the p-
 354 metastable point having a vertical tangent, that is, the point on
 355 the isotherm where $\theta = \theta_m$ (desorption branch) or $\theta = \theta_M$
 356 (adsorption branch): indeed, repeating the m-stability argu-
 357 ment, and letting θ move on a vertical tangent, then $\Delta\tilde{\mu}$ does
 358 not change sign when $\theta - \theta_m$ does. The m-instability of these
 359 points is important in interpreting the region of two-valuedness
 360 as a hysteresis loop with the following boundaries: its upper
 361 and lower boundaries coincide with the desorption and
 362 adsorption branches over a pressure interval $[\tilde{P}_1, \tilde{P}_2]$. \tilde{P}_2 is
 363 the abscissa of the point on the adsorption branch whose
 364 ordinate is the left spinodal coverage, θ_M , whereas \tilde{P}_1 is the
 365 abscissa of the point on the desorption branch whose ordinate
 366 is the right spinodal coverage, θ_m . Note that the left and right
 367 boundaries of the hysteresis loop can only be the vertical lines

368 at $\tilde{P} = \tilde{P}_1$ and $\tilde{P} = \tilde{P}_2$ because (\tilde{P}_1, θ_m) and (\tilde{P}_2, θ_M) are the only
 369 m-unstable points on the desorption and the adsorption
 370 branches: the transition to a mathematically and physically
 371 stable state can only take place from (\tilde{P}_2, θ_M) during
 372 adsorption, and from (\tilde{P}_1, θ_m) during desorption. See Figure
 373 2, right plot. Note also that the vertical boundaries of the
 374 hysteresis loop are not places of equilibrium, as these are in
 375 regions where $\Delta\tilde{\mu} \neq 0$. They are drawn as dashed lines in
 376 Figure 2 to emphasize this fact.

377 A further remark on the p-metastable states follows: by
 378 definition, a p-metastable adsorbate state will, if perturbed,
 379 transit to a p-stable state of lower energy. Referring to Figure
 380 14 (right), such a transition brings the adsorbate from a point
 381 on one of the green lines to the reconstructed dash-dotted line
 382 at the same value of coverage. This implies that it is not
 383 possible to say whether an equilibrium state represented by a
 384 point situated on one of the green lines of Figure 2 (right plot)
 385 is in a two-phase or in a one-phase adsorbate state: the two
 386 states have the same coverage and also the same ambient
 387 pressure. The equality of pressures is approximative and is due
 388 to the assumptions that characterize M' , implying that changes
 389 in the adsorbate are not "visible" in the ambient gas. As a
 390 consequence, p-stable and p-metastable adsorbate states are
 391 treated in the same way in Section 2.5 below.

392 Thus, for equilibrium isotherms that can be obtained from
 393 analytical expressions, model M' defines a subcritical
 394 equilibrium isotherm plotted against pressure as follows: it
 395 has an adsorption branch that spans all pressures up to a
 396 pressure \tilde{P}_2 at which the adsorbate is at its left spinodal
 397 coverage, θ_M . It has a desorption branch that spans pressures
 398 down to a pressure \tilde{P}_1 at which the adsorbate is at its right
 399 spinodal coverage θ_m . $\tilde{P}_1 < \tilde{P}_2$, hence, the interval $(\tilde{P}_1, \tilde{P}_2)$
 400 defines the pressure range of the hysteresis loop. The vertical
 401 boundaries of the loop at pressures \tilde{P}_1 and \tilde{P}_2 do not consist of
 402 equilibrium points.

403 Sections 2.4 and 2.5 look at supercritical and at subcritical
 404 isotherms in cases where no analytical solution is available, that
 405 is, when $\tilde{\mu}_{f,red}$ is given by eq 49 (left).

406 **2.4. Numerical Equilibrium Isotherms for Super-**
critical Adsorbates and Their Stability. Model M' is
 407 now considered for the general case of numerically solving eq 3
 408 for $\tilde{T} \geq \tilde{T}_{\Sigma c}$.

410 According to eq 56, the $\Delta\tilde{\mu}$ versus θ curve, at given r_e , \tilde{T} ,
 411 $\tilde{T}_{\Sigma c}$ and ψ , is the $\tilde{\mu}_{\Sigma,red}$ versus θ curve with a vertical translation
 412 induced by $\tilde{\mu}_{f,red}(r_e, \tilde{T})$ and by $\psi(\tilde{T})$. The $\tilde{\mu}_{\Sigma,red}$ versus θ curve
 413 has the shape of the monotonically increasing curve shown in
 414 Figure 15 (right). One can immediately conclude that there
 415 will always be a solution (as the curve spans the vertical axis
 416 from $-\infty$ to $+\infty$), and that it is unique. Using mathematical
 417 stability, as defined in Section 2.2, together with the plots of
 418 $\Delta\tilde{\mu}$ versus θ , one concludes that $\theta_e(r_e)$ is m-stable in addition
 419 to being p-stable. For later reference, this equilibrium solution
 420 is written as

$$\theta_e(r_e, \tilde{T}, \tilde{T}_{\Sigma c}, \psi) = \text{unique solution of eq 3,} \\ (\tilde{T} \geq \tilde{T}_{\Sigma c}) \quad (7)$$

422 Its general shape is given in Figure 2 (left).

423 The interpretation of eq 3 as the intersection with the θ -axis
 424 of a vertically translated $\tilde{\mu}_{\Sigma,red}$ versus θ curve has some useful
 425 consequences concerning the general shape of an equilibrium
 426 supercritical isotherm, especially the location of its point of
 427 inflection.

Knowing the set $\{\tilde{T}, \tilde{T}_{\Sigma c}, \psi\}$, it is possible to roughly predict 428
 the position of the region where the isotherm is steepest, 429
 assuming that the parameters in the set above are such that the 430
 isotherm flattens out. This follows from the observation that 431
 the $\tilde{\mu}_{\Sigma,red}$ versus θ curve can be translated upward by an 432
 arbitrary amount by letting r_e go arbitrarily close to 0. Letting 433
 r_e increase from such a value, the $\tilde{\mu}_{\Sigma,red}$ versus θ curve is 434
 translated downward, and its intersection with the θ axis gives 435
 values of θ_e that increase, the fastest increase taking place when 436
 the inflection point of the $\tilde{\mu}_{\Sigma,red}$ versus θ curve is close to the θ - 437
 axis. This can only happen if ψ (the other quantity that is 438
 subtracted from $\tilde{\mu}_{\Sigma,red}$ in the expression of $\Delta\tilde{\mu}$) is large enough. 439
 It is then useful to define a function $\Psi_u(\tilde{T}, \tilde{T}_{\Sigma c})$ as follows: if ψ 440
 $= \Psi_u$, then the inflection point of the $\Delta\tilde{\mu}$ versus θ curve, at 441
 given \tilde{T} , $\tilde{T}_{\Sigma c}$, and at $r = r_g(\tilde{T})$, is on the θ -axis. The inflection 442
 point, easily found by equating to zero the second derivative of \tilde{T} 443
 $\tilde{\mu}_{\Sigma,red}$ with respect to θ , occurs at $\theta = 1/3$, independently of \tilde{T} 444
 and of $\tilde{T}_{\Sigma c}$, so that 445

$$\Psi_u(\tilde{T}, \tilde{T}_{\Sigma c}) = \tilde{\mu}_{\Sigma,red}(1/3, \tilde{T}, \tilde{T}_{\Sigma c}) - \tilde{\mu}_{f,red}(r_g(\tilde{T}), \tilde{T}) \quad (8) \quad 446$$

See Figure 4 for the general behavior of Ψ_u . Note that Ψ_u 447
 does not depend on the values in the set \mathcal{D} . 448

Figure 3, shows how the shape of the equilibrium isotherm 449 B
 changes for values of ψ in the neighborhood of Ψ_u . Note that 450
 the tendency toward flattening occurs when $\psi > \Psi_u$. 451

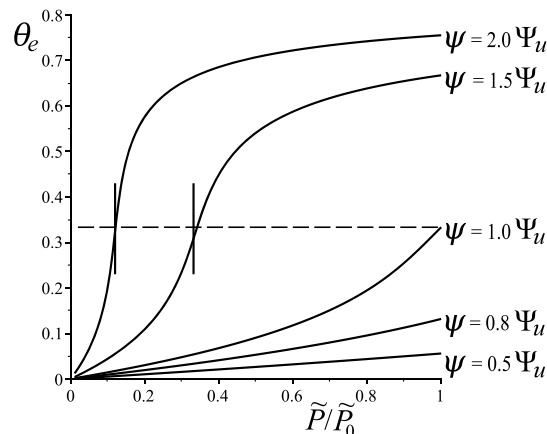


Figure 3. Equilibrium supercritical isotherms, θ_e vs \tilde{P}/\tilde{P}_0 , where $\tilde{T}_{\Sigma c} =$
 0.5 and $\tilde{T} = 0.6$. Curves originate from eq 7. The value of ψ is
 indicated for each curve ($\Psi_u = 1.2188$). The horizontal dashed line is
 at $\theta_e = 1/3$. Concerning the vertical segments, see the end of Section
 2.4.

On an equilibrium isotherm plotted as θ_e versus r_e , one can 452
 find the approximate position of its point of inflection. It is the 453
 value of r_e , here denoted r_i , that corresponds to $\theta_e = 1/3$. 454
 According to eq 4, it is given by 455

$$\tilde{r}_i(r_i, \tilde{T}) = e^{-\psi/\tilde{T}} \tilde{r}_{\Sigma}(\tilde{T}, \tau) \quad (9) \quad 456$$

One can obtain a good approximation for this r_i if one can 457
 assume that it is sufficiently close to 0 that $\tilde{r}_i \approx \tilde{T}r_i$ (see eq 47 458
 (right)). Then, using eq 46 (right), one gets 459

$$r_i = \frac{e^{1/2-9/4\tau}}{2} e^{-\psi/\tilde{T}} = \frac{e^{1/2-9/4\tau}}{2\tilde{K}_H} \quad (10) \quad 460$$

In Figure 3, the values of $\tilde{T}r_i/\tilde{P}_0$ given by this expression for 461
 $\psi = 1.5\Psi_u$ and $2.0\Psi_u$ are indicated by the vertical segments. 462

463 **2.5. Numerical Equilibrium Isotherms for Subcritical**
 464 **Adsorbates and Their Stability.** Returning to the
 465 interpretation of eq 3 as the intersection with the θ -axis of a
 466 vertically translated $\tilde{\mu}_{\Sigma,\text{red}}$ versus θ curve, one now assumes $\tilde{T} <$
 467 $\tilde{T}_{\Sigma c}$, so that the $\tilde{\mu}_{\Sigma,\text{red}}$ versus θ curve has a local maximum and a
 468 local minimum as shown in Figure 15 (right). There can now
 469 be one, two, or three values of θ_e , depending on the position of
 470 the $\Delta\tilde{\mu}$ versus θ curve in relation to the θ -axis. This position
 471 depends, in turn, on the values of $\tilde{\mu}_{f,\text{red}}$ and ψ .

472 The use of mathematical stability in this case leads to the
 473 following. If there is just one value of θ_e , then it occurs as the
 474 intersection with the θ -axis of that part of the translated $\tilde{\mu}_{\Sigma,\text{red}}$
 475 versus θ curve that is either to the left of the local maximum or
 476 to the right of the local minimum and is therefore m-stable. If
 477 there are two distinct values of θ_e , then one of them is m-
 478 stable, the other (being the abscissa of the local maximum or
 479 minimum) is m-unstable and discarded. If there are three
 480 values of θ_e , then: (i) the smallest and largest are m-stable,
 481 whereas the middle one is m-unstable and discarded; (ii) the
 482 smallest is in the interval $(0, \theta_M)$, and the largest is in the
 483 interval $(\theta_m, 1)$.

484 For later reference, the m-stable equilibrium solutions are
 485 written

$$486 \quad \theta_{ea}(r_e, \tilde{T}, \tilde{T}_{\Sigma c}, \psi) = \text{solution of eq 3 in } (0, \theta_M),$$

$$(\tilde{T} < \tilde{T}_{\Sigma c}) \quad (11)$$

$$487 \quad \theta_{ed}(r_e, \tilde{T}, \tilde{T}_{\Sigma c}, \psi) = \text{solution of eq 3 in } (\theta_m, 1),$$

$$(\tilde{T} < \tilde{T}_{\Sigma c}) \quad (12)$$

488 Because $\theta_M < \theta_m$, there are two separate branches as in
 489 Section 2.3, an adsorption branch, θ_{ea} , and a desorption
 490 branch, θ_{ed} , creating a double-valuedness for certain pressures.
 491 As in the right plot of Figure 2, this is interpreted to mean that
 492 there is a hysteresis loop and a phase transition for the
 493 adsorbate.

494 The sizes of ψ and of r_g being important, one is led to define
 495 the following two functions of \tilde{T} and $\tilde{T}_{\Sigma c}$

$$496 \quad \Psi_m(\tilde{T}, \tilde{T}_{\Sigma c}) = \tilde{\mu}_{\Sigma,\text{red}}(\theta_m, \tilde{T}, \tilde{T}_{\Sigma c}) - \tilde{\mu}_{f,\text{red}}(r_g, \tilde{T}) \quad (13)$$

$$497 \quad \Psi_M(\tilde{T}, \tilde{T}_{\Sigma c}) = \tilde{\mu}_{\Sigma,\text{red}}(\theta_M, \tilde{T}, \tilde{T}_{\Sigma c}) - \tilde{\mu}_{f,\text{red}}(r_g, \tilde{T}) \quad (14)$$

498 where θ_m and θ_M are as defined in Figures 14 and 15, and by eq
 499 37. It is easily seen that $\Psi_m < \Psi_M$. Both functions depend on \tilde{T}
 500 and $\tilde{T}_{\Sigma c}$ and not on the set \mathcal{D} . Figure 4 shows the behavior of
 501 Ψ_m , Ψ_M , and Ψ_u versus \tilde{T} for $\tilde{T}_{\Sigma c} = 0.5$.

502 It is now clear that the shape of an isotherm critically
 503 depends on the value of ψ . To make a more detailed
 504 description, plots of $\Delta\tilde{\mu}(\theta, r, \tilde{T}, \tilde{T}_{\Sigma c}, \psi)$ versus θ are shown in the
 505 third row of Figure 5, where the parameters are chosen as
 506 follows: $\tilde{T} = 0.4$, $\tilde{T}_{\Sigma c} = 0.5$; r is given its maximum value, $r_g(\tilde{T})$,
 507 consistent with the assumption that the ambient fluid is a gas;
 508 finally, $\psi < \Psi_m$ (left-hand plot), $\Psi_m < \psi < \Psi_M$ (center plot),
 509 and $\psi > \Psi_M$ (right-hand plot). Obviously, the value of ψ
 510 determines the position of the curve relative to the θ -axis, given
 511 that $r = r_g$.

512 One can now draw θ_e versus r_e for the three ψ -cases given
 513 above by gradually reducing r_e from r_g to 0 and getting the
 514 corresponding value(s) of θ_e . Graphically, this means trans-
 515 lating the curves shown in the third row vertically upward, and
 516 noting the values of θ_e at which the black lines cross the θ -axis;
 517 the intersection of the black line to the left gives θ_{ea} , whereas

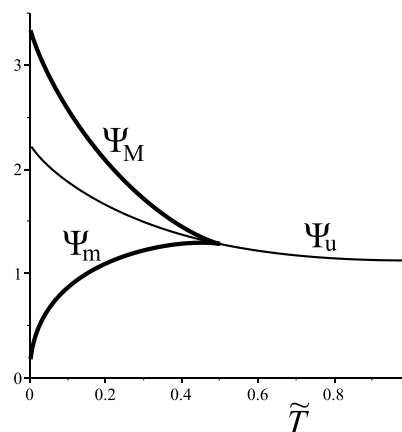


Figure 4. Special ψ 's versus dimensionless temperature, \tilde{T} . The upper thick line is Ψ_M defined by eq 14, the lower thick line is Ψ_m defined by eq 13, and the thin line is Ψ_u defined by eq 8. The first two are defined for $0 < \tilde{T} < \tilde{T}_{\Sigma c}$, whereas the last is defined for $\tilde{T} > 0$. All curves are drawn with $\tilde{T}_{\Sigma c} = 0.5$.

the black line to the right gives θ_{ed} . Numerically, by using eqs 518 11 and 12. Functions θ_{ea} and θ_{ed} plotted against r_e or, 519 equivalently against the pressure, are shown as solid lines in the 520 fourth row of Figure 5. It is graphically obvious that θ_{ed} does 521 not exist for the case $0 < \psi < \Psi_m$, and that both θ_{ea} and θ_{ed} 522 exist for larger ψ -values, albeit for a limited range for r or P 523 values. The dotted lines that connect the desorption and the 524 adsorption branches are the isotherms given by eq 6. See, for 525 comparison, the right plot in Figure 2, and note, in particular 526 that $\tilde{P}(r_1, \tilde{T}) = \tilde{P}_1$ and that $\tilde{P}(r_2, \tilde{T}) = \tilde{P}_2$. 527

One sees that the adsorption branches, shown in the fourth 528 row, only reach the value $r = r_2 < r_g$ if ψ is large enough that 529 the local maximum of the $\Delta\tilde{\mu}$ versus θ curve is below the θ -axis 530 when $r = r_g$, so that lifting the curve by reducing r brings the 531 local maximum on the θ -axis when $r = r_2$: see the third column 532 of the fourth row. Note also that, when this occurs, the 533 adsorption branch stops being defined and that it seems to 534 have a vertical tangent at $r = r_2$. Similar statements hold for the 535 desorption branch. 536

The statements that the adsorption branch stops at r_2 , 537 whereas the desorption branch stops at r_1 , both with vertical 538 tangents, are correct because an equilibrium isotherm is a curve 539 satisfying $\tilde{\mu}_{\Sigma,\text{red}}(\theta_e, \tilde{T}, \tilde{T}_{\Sigma c}) - \tilde{\mu}_{f,\text{red}}(r_e, \tilde{T}) - \psi = 0$, whose 540 tangents are given by 541

$$\frac{d\theta_e}{dr_e} = \frac{\partial\tilde{\mu}_{f,\text{red}}/\partial r_e}{\partial\tilde{\mu}_{\Sigma,\text{red}}/\partial\theta_e}$$

Thus, the local extrema of the $\tilde{\mu}_{\Sigma,\text{red}}$ versus θ curve produce 542 vertical tangents on the isotherms, and there is agreement with 543 the case of the analytical equilibrium isotherms, Section 2.3. 544 The agreement goes, in fact, deeper because it is possible to 545 repeat the stability analysis of Section 2.3 for the isotherms, 546 and also for the points with vertical tangents, with the same 547 conclusions. 548

It is now possible to interpret the multivaluedness in the 549 equilibrium isotherms, by introducing a hysteresis loop. 550

Referring first to the plots of the third column, fourth and 551 fifth rows of Figure 5, one interprets the two-valuedness of 552 coverage as in Section 2.3: there is an adsorption curve 553 $abcd\beta\alpha$, and a desorption curve $a\beta\gamma\delta\beta a$. As pointed out in 554

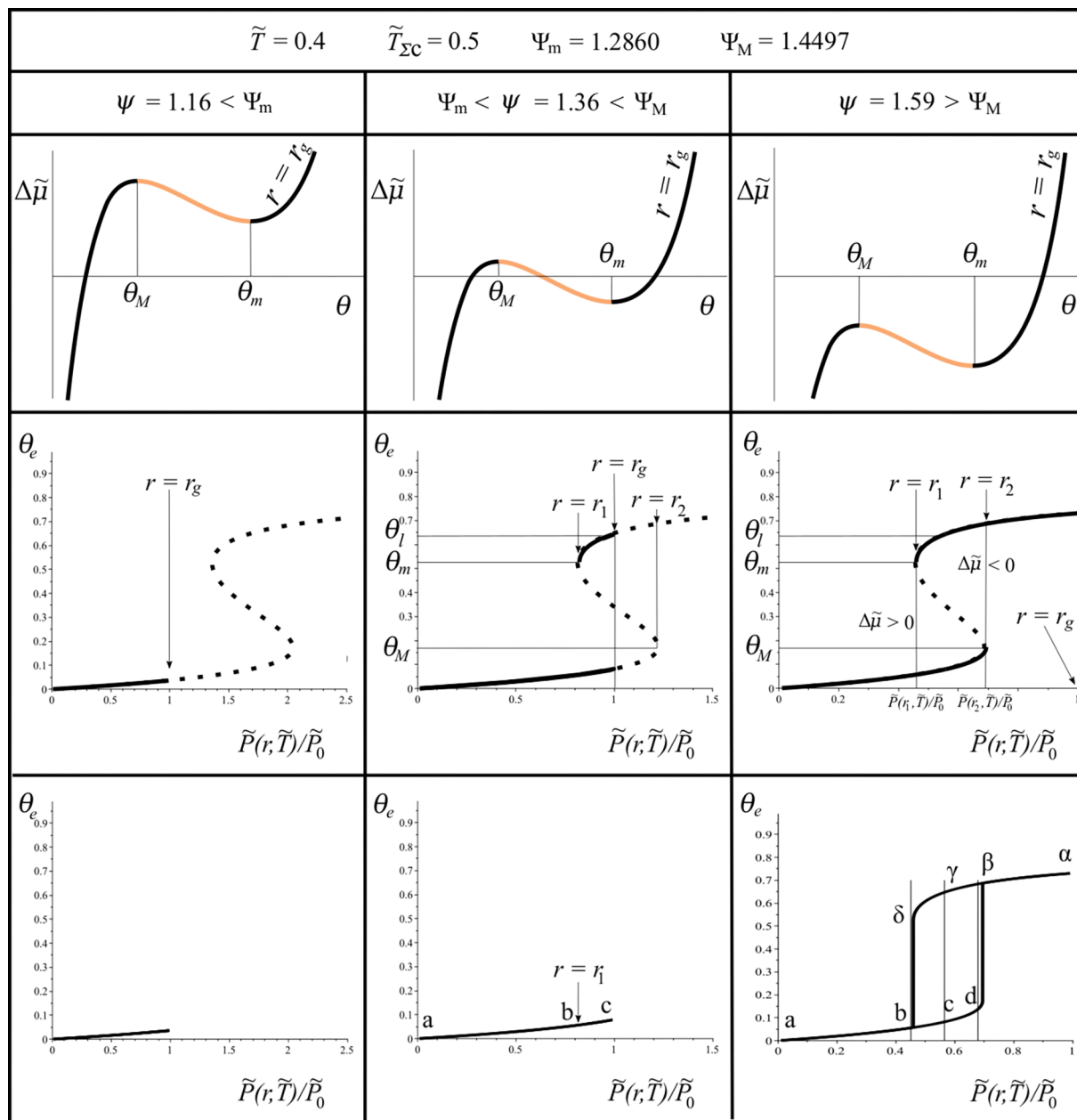


Figure 5. Illustrating the numerical calculation of equilibrium isotherms for subcritical temperatures. All plots are done with $\tilde{T} = 0.4$ and $\tilde{T}_{\Sigma c} = 0.5$. The values of ψ are, column-wise: $\psi < \Psi_m$ (left), $\Psi_m < \psi < \Psi_M$ (center), and $\psi > \Psi_M$ (right). For the plots of the third row, it is reminded that $\Delta\tilde{\mu} = \tilde{\mu}_{\Sigma, \text{red}}(\theta, \tilde{T}, \tilde{T}_{\Sigma c}) - \tilde{\mu}_{f, \text{red}}(r, \tilde{T}) - \psi(\tilde{T}, \mathcal{D})$. See text in Section 2.5, after eq 14.

555 Section 2.3, no solution of eq 11 or of eq 12 will be situated on
 556 one of the vertical boundaries of the hysteresis loop $bcd\gamma\delta$.
 557 The ambient densities r_1 and r_2 , identifying the left and right
 558 boundaries of the hysteresis loop (see the fourth row in Figure
 559 5) are functions of \tilde{T} , $\tilde{T}_{\Sigma c}$, and ψ , easily calculable by the
 560 following expressions

$$r_1 = x \in (0, r_g) \text{ such that } \Delta\mu(\theta_m, x, \tilde{T}, \tilde{T}_{\Sigma c}, \psi) = 0, \quad (\psi > \Psi_m) \quad (15)$$

$$r_2 = x \in (0, r_g) \text{ such that } \Delta\mu(\theta_M, x, \tilde{T}, \tilde{T}_{\Sigma c}, \psi) = 0, \quad (\psi > \Psi_M) \quad (16)$$

Turning now to the plots of the second column, fourth and fifth rows of Figure 5, it is seen that the upper solid line of the hysteresis loop must be discarded as a possible equilibrium isotherm, at least if one assumes that desorption occurs after adsorption, because adsorption stops before the mathematically unstable point (where $\theta = \theta_M$) is reached, and the adsorbate has not transited to the desorption branch. Adsorption occurs along abc , stops at c because of the $\tilde{P} < \tilde{P}_0$ condition, and then desorption follows the adsorption branch but in the reverse direction, that is, along cba .

An important conclusion follows: there are two main classes for the values of ψ : the class $\psi \leq \Psi_M$ in which the isotherms show low coverage and are structureless (fifth row, left-hand and center plots in Figure 5) and the class $\psi > \Psi_M$ in which the

577 isotherms show an adsorbate phase transition and a hysteresis
578 loop (fifth row, right-hand plot).

579 When $\psi > \Psi_M$, it is of some interest to predict the
580 approximate pressure of the center of the loop, and also the
581 pressures of its left and right vertical boundaries. The pressure
582 in the approximate middle of the loop is $\tilde{P}(r_i, \tilde{T})$ where r_i is the
583 previously found density at which the ambient chemical
584 potential has an inflection point, see eq 10. The pressures
585 approximating the left and right vertical boundaries are $\tilde{P}(r_1, \tilde{T})$
586 and $\tilde{P}(r_2, \tilde{T})$ where approximate expressions can be found for r_1
587 and r_2 in a manner similar to the one that led to eq 10.
588 Equations 15, and 16 are equivalent to

$$\begin{aligned}\tilde{f}_\Sigma(\theta_m, \tilde{T}, \tau) &= \tilde{K}_{Hf} \tilde{f}_i(r_1, \tilde{T}), \\ \tilde{f}_\Sigma(\theta_M, \tilde{T}, \tau) &= \tilde{K}_{Hf} \tilde{f}_i(r_2, \tilde{T})\end{aligned}$$

589 and assuming that r_1 and r_2 are small, one finds

$$\begin{aligned}r_1(\tilde{T}, \tilde{T}_{\Sigma c}, \psi) &= E_m(\tau) e^{-\psi/\tilde{T}} = \frac{E_m(\tau)}{\tilde{K}_H}, \\ r_2(\tilde{T}, \tilde{T}_{\Sigma c}, \psi) &= E_M(\psi) e^{-\psi/\tilde{T}} = \frac{E_M(\tau)}{\tilde{K}_H}\end{aligned}\quad (17)$$

591 where

$$E_m(\tau) = \frac{\tilde{f}_\Sigma(\theta_m, \tilde{T}, \tau)}{\tilde{T}} = \frac{\theta_m}{1 - \theta_m} \exp\left(\frac{\theta_m}{1 - \theta_m} - \frac{27}{4} \frac{\theta_m}{\tau}\right)\quad (18)$$

592 (E_M being obtained from above by substituting M to m) and
593 where θ_m and θ_M are the functions of τ given by eq 37.

594 In the same approximation for which the above expressions
595 are valid (low values of r), one can write the width of the
596 hysteresis loop, in units of pressure, as $w = 8P_c \tilde{T}(r_2 - r_1)$ (see
597 eq 33, right), that is

$$\begin{aligned}w &= 8P_c \tilde{T} [E_M(\tau) - E_m(\tau)] e^{-\psi/\tilde{T}} \\ &= \frac{8P_c \tilde{T} [E_M(\tau) - E_m(\tau)]}{\tilde{K}_H}\end{aligned}\quad (19)$$

600 $E_M - E_m$ versus τ is shown in Figure 6. The three pressures
601 $\tilde{P}(r_i, \tilde{T})$, $\tilde{P}(r_1, \tilde{T})$, and $\tilde{P}(r_2, \tilde{T})$ are indicated by vertical lines on
602 the plot of the fifth row and third column in Figure 5.

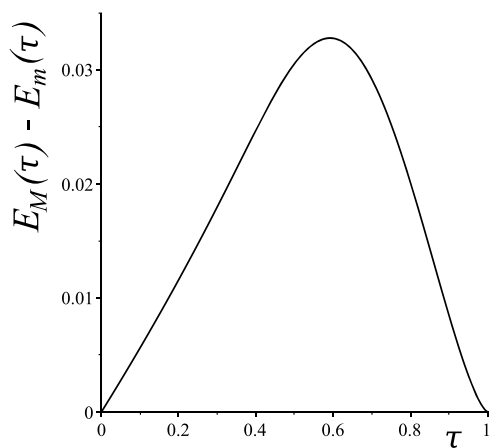


Figure 6. For $\tau = \tilde{T}/\tilde{T}_{\Sigma c} < 1$, the width of the hysteresis loop is proportional to $E_M - E_m$ (see eq 19), a function of τ that vanishes at $\tau = 0$ and $\tau = 1$. Its maximum, 0.03281 is attained when $\tau = 0.5917$.

3. RESULT AND DISCUSSION 2: THEORY OF TIME-DEPENDENT ISOTHERMS

603

Time-dependent solutions of eq 59 are now considered, that
604 simulate the thought experiment described in the next
605 paragraph below, leading to a description of dynamical
606 isotherms, and to their behavior in relation to equilibrium
607 isotherms and to hysteresis loops. Two subcases are
608 considered: the supercritical and the subcritical adsorbate. It
609 is believed that the actual values of \tilde{T} and $\tilde{T}_{\Sigma c}$ are of secondary
610 importance as compared to their relative sizes. $\tilde{T}_{\Sigma c} = 0.5$ has
611 been used repeatedly above, and is also used in what follows,
612 whereas $\tilde{T} = 0.6$ and $\tilde{T} = 0.4$ are used for the two cases.

The thought-experiment considered is as follows. An
614 amount of mesoporous or macroporous medium is placed in
615 a container filled with a one-component gas at low pressure P
616 and at uniform constant temperature T , which is less than the
617 critical temperature. After the gas in the pores has settled into a
618 state of zero velocity and uniform pressure P_i , which is less
619 than the saturation pressure P_0 , the pressure in the gas is slowly
620 increased to a pressure $P_f \leq P_0$, then slowly decreased back to
621 P_i . Recordings of the amounts adsorbed, and of the
622 corresponding ambient densities or pressures are assumed to
623 occur continuously. The duration of the cycle $P_i \rightarrow P_f \rightarrow P_i$ is
624 assumed to be large enough for the ambient density to remain
625 nearly uniform, and for the ambient velocity to be nearly zero,
626 in the macroporous medium at all times. (See the description
627 of model M' in the Introduction.)

The cycle of applied pressure forces the ambient density to
629 follow a similar cycle. In M' , $r(\tilde{t})$ is needed as extra input to
630 solve eq 59. Mathematically, one can introduce a function $\tilde{P}(\tilde{t})$
631 and find the resulting $r(\tilde{t})$ by solving the equation of state. A
632 simplification is described in what follows, that avoids time-
633 consuming calculations by starting directly with a function $r(\tilde{t})$
634 that goes through a cycle, starting from a low-value r_e ,
635 increasing to a high-value $r_i \leq r_g$, then decreasing back to r_e .
636 Such a function is shown in Figure 7, where the increasing and
637 17

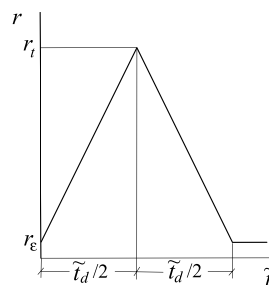


Figure 7. Function $r(\mathcal{P}; \tilde{t})$, where \mathcal{P} is the set of three parameters $\{r_e, r_i, \tilde{t}_d\}$. The function simulates a compression–decompression cycle.

decreasing parts are linear. The minimum r_e is introduced so as
638 to avoid the singularity of the chemical potential at $r = 0$, and a
639 value $r_e = r_i/10^3$ is in general sufficient. The figure defines
640 $r(\mathcal{P}; \tilde{t})$, where \mathcal{P} is the set of three parameters $\{r_e, r_i, \tilde{t}_d\}$. The
641 time parameter, \tilde{t}_d will be called the cycle duration.

Equation 59 is solved^b with an initial condition, 642
643 $\theta(0) = r(\mathcal{P}; 0) \exp(\psi/\tilde{T})$. Concerning the arguments of $\Delta\tilde{\mu}$,
644 $r(\mathcal{P}; \tilde{t})$ is substituted to r and, as already mentioned, $\tilde{T}_{\Sigma c} = 0.5$
645 and two values are considered for \tilde{T} , that is 0.4 and 0.6. The
646 central purpose of the calculations is to determine the
647 influence of the values of ψ and of the cycle duration \tilde{t}_d on
648 the shapes of the time-dependent isotherms.

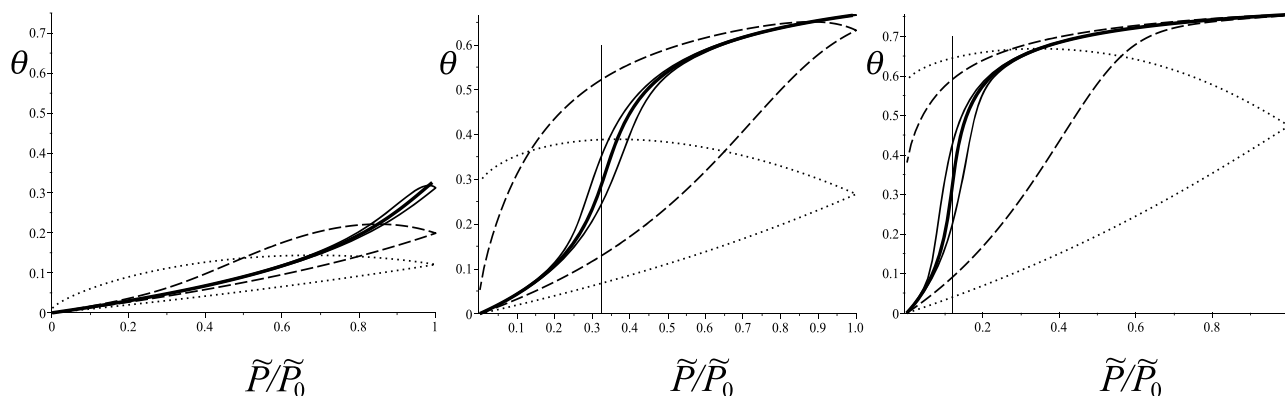


Figure 8. Isotherms for a supercritical adsorbate: $\tilde{T}_{\text{Sc}} = 0.5$, $\tilde{T} = 0.6$. The values of ψ are, from the left to the right plot, equal to $\Psi_u = 1.22$, $1.5\Psi_u = 1.83$, and $2.0\Psi_u = 2.44$. The thick solid line is the equilibrium isotherm in each plot. For all plots, the values of the loop duration \tilde{t}_d are: 1 for the dotted lines, 5 for the dashed lines, and 100 for the solid lines. The vertical thin lines are at $P(r_i, \tilde{T})$.

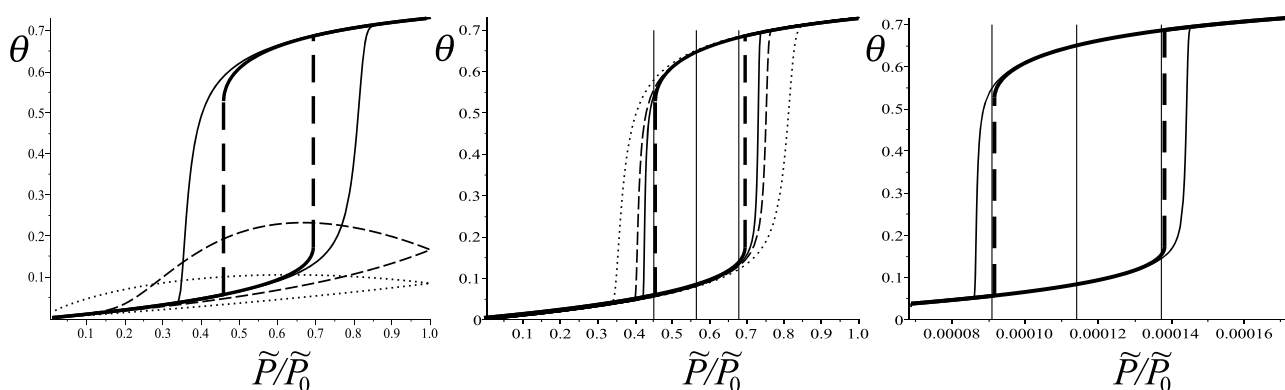


Figure 9. Isotherms for a subcritical adsorbate. For all three plots, $\tilde{T}_{\text{Sc}} = 0.5$, $\tilde{T} = 0.4$, the thick solid lines are the equilibrium isotherms, and the thick dashed lines are the hysteresis boundaries. Left plot: $\psi = 1.1\Psi_M = 1.595$; dynamic isotherms calculated with $r_e = 0.01r_g$, $r_t = r_g$, $\tilde{t}_d = 1$ (thin dotted), 5 (thin dashed), 100 (thin solid). Center plot: $\psi = 1.1\Psi_M = 1.595$; $r_e = 0.01r_g$, $r_t = r_g$, $\tilde{t}_d = 100$ (thin dotted), 300 (thin dashed), 600 (thin solid). Right plot: $\psi = 5$; dynamic isotherm calculated with $r_e = 0.75r_1$, $r_t = 1.25r_2$, $\tilde{t}_d = 600$ (thin solid). In the center and right plots, the vertical thin lines are placed at $r = r_1$, r_i , r_2 .

647 The supercritical case is examined first, and $\tilde{T} = 0.6$ is used.

648 **Figure 8** shows the results obtained as three plots, with four
649 curves in each plot, and increasing values of ψ from left to right
650 (based on the case of the equilibrium isotherms of [Section](#)
651 [2.4](#)). In each plot, the thick-lined curve is the equilibrium
652 isotherm, and the other curves are dynamic isotherms with
653 increasing cycle times, \tilde{t}_d as indicated in the caption. The
654 vertical thin lines are at the approximate positions of the
655 inflection points of the equilibrium isotherms, given by [eq 10](#).
656 The most noticeable feature is exhibited by the dotted-line
657 isotherms (short cycle duration), where adsorption increases
658 long after the start of decompression. Also remarkable is the
659 tendency of the isotherms to exhibit loops that resemble
660 hysteresis loops found in magnetism, but that shrink when the
661 cycle duration increases. This type of hysteresis was apparently
662 first observed in piezoelectric measurements in 2003 and
663 denoted then as rate-dependent hysteresis.¹⁶

664 Both features above are experimentally observed in
665 adsorption, as shown in the review article by Wang et al.⁹
666 For further discussion, see [Section 4](#).

667 The subcritical case is now examined, and $\tilde{T} = 0.4$ is used,
668 with $\tilde{T}_{\text{Sc}} = 0.5$.

669 According to the conclusion drawn in [Section 2.5](#), one can
670 concentrate on cases where the equilibrium isotherms show
671 phase transition and hysteresis, that is, the cases $\psi > \Psi_M$. The
672 three plots in [Figure 9](#) show equilibrium isotherms, vertical

hysteresis boundaries, and dynamic isotherms resulting from
various cycle durations, as indicated in the caption.

The dynamical isotherms in the left plot are calculated with
the same cycle durations, \tilde{t}_d , used for the dynamical isotherms
in [Figure 8](#). They show, for small cycle durations, the same
increase in adsorption even after the start of decompression.
The center plot shows the tendency of the dynamical
isotherms to approach the equilibrium isotherms when the
cycle duration increases. In particular, the left and right
boundaries of the hysteresis loop seem to attract the parts of
the time-dependent isotherms that join low to high (or, for
decompression, high to low) density adsorbate. However, the
vertical hysteresis boundaries are not places of equilibrium, and
the reason for the behavior of the time-dependent isotherms is
that they are forced toward a vertical direction by being
attracted to the parts of the upper and lower boundaries that
rapidly curve from the near horizontal to the vertical.

The right plot, with $\psi = 5$, simulates conditions of high
adsorption (see [Figure 16](#)). The notable fact here is that the
phase transition and accompanying hysteresis loop happen at
very low pressures, the width of the loop also being quite small.
The center and right plots show that the placement and width
of the loop are well described by r_i , r_1 , and r_2 , given by [eqs 10](#)
and [17](#).

4. RESULT AND DISCUSSION 3: REINTERPRETING THE SORPTION OF CO₂ AND CH₄ ON COAL

697
698 A number of publications (Zhao et al.⁶ and refs 15–28 given
699 there) report experiments of methane and carbon dioxide
700 sorption, showing isotherms with hysteresis loops at temper-
701 atures where capillary condensation cannot explain the
702 hysteresis.^{6,9} In fact, these isotherms have loops that bear a
703 strong resemblance to the one presented in Section 3,
704 especially in Figure 8. One of these experiments is examined
705 below in the framework of model M'.

706 The experiment in question is the one reported by Jessen et
707 al.⁷ It is here interpreted in a way that differs from the one
708 given by the authors. Shortly stated, the authors fit one static
709 isotherm to the adsorption data and another to the desorption
710 data (both are Langmuir isotherms), thus obtaining two
711 separate values for the Henry adsorption constant, one for
712 adsorption and one for desorption. In model M', however, it is
713 possible to fit just one time-dependent isotherm to the set of
714 data consisting of adsorption and desorption, and thus obtain a
715 unique Henry constant. More precisely, M' has two internal
716 parameters, $\tilde{T}_{\Sigma c}$ and μ . However, fitting an isotherm to the data
717 requires, as shown below, the introduction of three additional
718 parameters. The least squares principle is applied, whereby the
719 best values of the parameters are the ones that minimize the
720 sum of the squared differences between the measured and
721 calculated values.

722 The raw data reported by Jessen et al.⁷ concerning the
723 adsorption–desorption at $T_{\text{exp}} = 295.15$ K of CO₂ by
724 Wyoming coal, are shown plotted in Figure 10. Points are

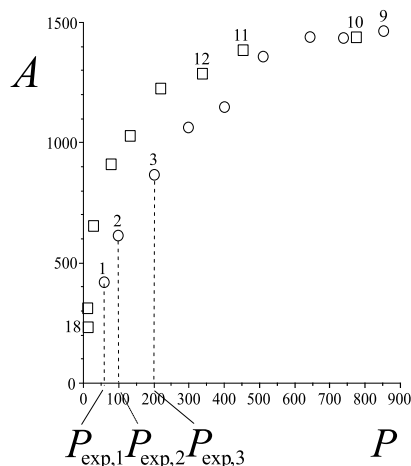


Figure 10. Adsorption (circles) and desorption (squares) of CO₂ by Wyoming coal at 295.15 K, as reported by Jessen et al.⁷ The horizontal axis gives pressure in PSI. The vertical axis gives the amounts adsorbed, A , in SCF per ton of coal. For the numbering of the points, see the text.

725 numbered in increasing order for increasing (adsorption), and
726 then decreasing (desorption) coverage. The coordinates of
727 point i are denoted $(P_{\text{exp},i}, A_{\text{exp},i})$ where, for the adsorption
728 points, $i = 1, \dots, N_a$ and for the desorption points, $i = N_a + 1, \dots,$
729 $N_a + N_d$, and $N_a = N_d = 9$. The amounts adsorbed are given in
730 SCF per ton of coal.

731 According to the NIST database, the critical temperature
732 and pressure for CO₂ are

$$T_{fc} = 304.2 \text{ K}, \quad P_c = 7.38 \times 10^6 \text{ Pa} = 0.1070 \times 10^4 \text{ PSI} \quad (20) \quad 733$$

The dimensionless temperature attached to the raw data of
734 Figure 10 is thus $\tilde{T}_{\text{exp}} = T_{\text{exp}}/T_{fc} = 295.2/304.2 = 0.9704$. 735

The ambient CO₂ is thus slightly subcritical. Assuming an
736 adsorbate critical temperature of about a half or less of the
737 above T_{fc} , one concludes that the adsorbate is supercritical.
738 According to model M', if hysteresis is observed, it must be of
739 one of the types drawn with a thin dashed or thin solid line on
740 the right-hand plot in Figure 8. In other words, it can only be a
741 rate-dependent hysteretic isotherm with a large value of t_r so
742 that its shrinking to the unique curve representing the
743 equilibrium isotherm is difficult to observe. 744

The experiment⁷ is described as follows. Adsorption is
745 driven by a series of compressions and relaxations, starting
746 from an initial low pressure $P_{\text{exp},1}$ and leading to a maximum
747 pressure $P_{\text{exp},9}$, which is less than saturation pressure (about
748 950 PSI at 295.15 K); desorption then follows, as a series of
749 decompressions and relaxations leading back to a low pressure
750 approximately equal to $P_{\text{exp},18}$. The compression and
751 decompression times are not given explicitly, but it is indicated
752 that relaxation times are of at least 24 h. 753

In the framework of model M', a simplified simulation of the
754 experiment consists of solving eq 59, with a function $r(\tilde{t})$ that
755 is not the simple compression–decompression cycle of Figure
756 7 but a cycle that includes a series of compressions and
757 relaxations followed by a series of decompressions and
758 relaxations, as shown in Figure 11. One then obtains 759 11

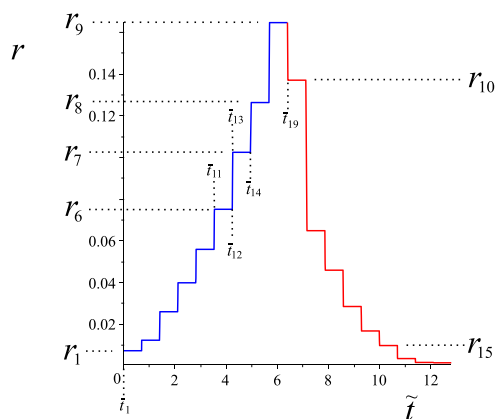


Figure 11. Function $r(\tilde{t})$ that simulates a series of compressions (the nearly vertical segments) and relaxations (the horizontal segments) followed by a series of decompressions and relaxations that lead to the measurement of the amounts of CO₂ adsorbed in the experiment by Jessen et al.⁷ (their Figure 2). See the text in Section 4 for the construction of this function.

theoretical coverage θ , as a dimensionless number between 0
760 and 1, in terms of dimensionless time \tilde{t} . Parametric plots of θ
761 versus r , with parameter \tilde{t} , can then be obtained. Recordings of
762 theoretical coverage and ambient density are made immedi-
763 ately after compression (in adsorption) or decompression (in
764 desorption), with the purpose of comparing them to the
765 experimental points $(P_{\text{exp},i}, A_{\text{exp},i})$. Two subsidiary problems
766 must obviously be solved: the first one is the same as
767 mentioned in the third paragraph of Section 3, of going from
768 pressure to density and back, and is solved by creating an array,
769 $r_{\text{exp},i}$ ($i = 1, \dots, N_a + N_d$), with elements satisfying $\tilde{P}(r_{\text{exp},i}, \tilde{T}_{\text{exp}}) = 770$

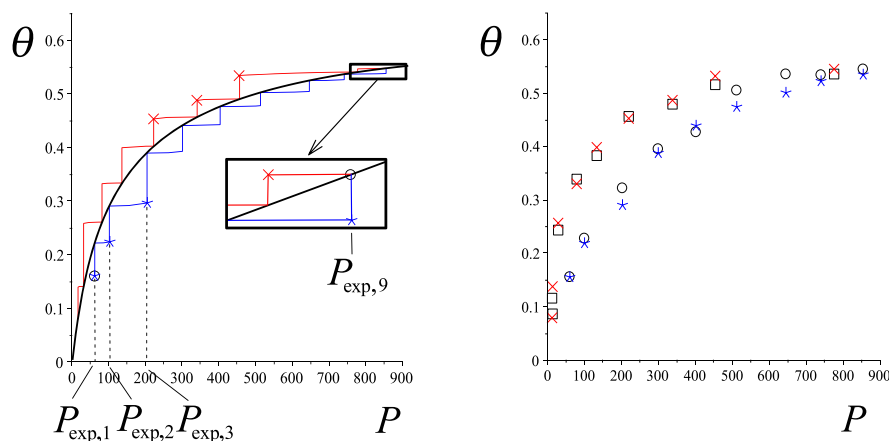


Figure 12. Interpretation of the experimental data shown in Figure 10. In both plots, the vertical axis gives dimensionless coverage; the horizontal axis gives ambient pressure in PSI. Left-hand plot: The smooth black curve is the theoretical equilibrium isotherm given by eq 7. The blue and red sawtooth curves, joined as shown in the inset, constitute the solution of eqs 23 and 24, the two colors referring to the colors in Figure 11. Asterisks and crosses indicate values to be compared to the measurements, see the right-hand plot. Right-hand plot: Circles and squares are the experimental data of Figure 10 for adsorption (circles) and desorption (squares) of CO₂ by Wyoming coal at 295.15 K.⁷ Blue asterisks (adsorption) and red crosses (desorption) result from model calculations as indicated by the left-hand plot.

774 $\tilde{P}_{\text{exp},i}$. The second is writing the experimental adsorptions $A_{\text{exp},i}$
 775 as dimensionless numbers $\theta_{\text{exp},i}$ between 0 and 1. To solve this
 776 second problem, one introduces a constant C , defined as

$$774 \quad \theta_{\text{exp},i} = A_{\text{exp},i}/C, \quad (i = 1, \dots, N_a + N_d) \quad (21)$$

775 For the determination of C , see item 3 in the algorithm
 776 below.

777 The simulation consists of several parts that are now
 778 described in more detail.

779 The first part is the construction of the function $r(\bar{t})$ shown
 780 in Figure 11. It is done as follows.

781 It is assumed that a recording of $(P_{\text{exp},i}, A_{\text{exp},i})$ for some value
 782 of i is followed by a relaxation time that is large enough for the
 783 adsorbate coverage to reach its equilibrium value. Relaxation is
 784 followed by a compression (or a decompression) that brings
 785 pressure $P_{\text{exp},i}$ to $P_{\text{exp},i+1}$ (equivalently, $r_{\text{exp},i}$ to $r_{\text{exp},i+1}$) and to the
 786 recording of $A_{\text{exp},i+1}$.

787 To minimize the number of parameters to be determined, it
 788 is assumed that the same relaxation time is used for all i , so that
 789 one relaxation time, \mathcal{R} , is introduced as a parameter to
 790 determine. Note, incidentally, that in theory, it takes infinite
 791 time to reach equilibrium so that \mathcal{R} must be such that
 792 equilibrium is reached within a certain acceptable tolerance.
 793 See item 4 in the algorithm below.

794 Another parameter to determine is introduced: a time
 795 variable, C , used to quantize the rate of compression/
 796 decompression. Let C be the estimated time that is necessary
 797 to carry out the compression of the ambient gas from the
 798 lowest pressure, $P_{\text{exp},1}$, to the highest adsorption pressure, $P_{\text{exp},9}$,
 799 at a constant rate. Then, the rate of compression can be
 800 obtained as

$$801 \quad v = (r_{\text{exp},N_a} - r_{\text{exp},1})/C \quad (22)$$

802 and the assumption is made that this rate is used to compress
 803 or decompress from any density to the next.

804 An array \bar{t}_i is then constructed, where the first value, \bar{t}_1 , is
 805 taken as the origin, assumed to be the time of the first data
 806 registration (labeled 1 in Figure 10); \bar{t}_2 is then the time at the
 807 end of the first relaxation. Then, \bar{t}_k , where $k = 3, \dots, 18$ are the
 808 successive times at the ends of the compressions and

relaxations leading to the last adsorbed value (labeled 9 in
 Figure 10) 809 810

$$\bar{t}_1 = 0,$$

$$\bar{t}_2 = \mathcal{R},$$

$$\bar{t}_{2n-1} = \bar{t}_{2n-2} + (r_{\text{exp},n} - r_{\text{exp},n-1})/v, \quad (n = 2, \dots, N_a),$$

$$\bar{t}_{2n} = \bar{t}_{2n-1} + \mathcal{R}, \quad (n = 2, \dots, N_a)$$

Times \bar{t}_k where k runs from 11 to 14 are shown in Figure 11. 811
 Also shown is the time of the first desorption, \bar{t}_{19} , at the end of 812
 the first decompression. The last registered desorption (labeled 813
 18 in Figure 10) is at \bar{t}_{36} 814

$$\bar{t}_{2N_a+2n-1} = \bar{t}_{2N_a+2n-2} + (r_{\text{exp},N_a+n-1} - r_{\text{exp},N_a+n})/v,$$

$$(n = 1, \dots, N_d),$$

$$\bar{t}_{2N_a+2n} = \bar{t}_{2N_a+2n-1} + \mathcal{R}, \quad (n = 1, \dots, N_d)$$

It is then useful to construct an array \bar{r} 815

$$\bar{r}_{2n-1} = r_n, \quad (n = 1, \dots, N_a + N_d),$$

$$\bar{r}_{2n} = r_n, \quad (n = 1, \dots, N_a + N_d)$$

so that the function $r(\bar{t})$ of Figure 11 is the function that joins 816
 point (\bar{t}_i, \bar{r}_i) to point $(\bar{t}_{i+1}, \bar{r}_{i+1})$ by a straight line, for $i = 1, \dots,$ 817
 $2N_a + 2N_d - 1$. 818

According to the description given above of the simplified 819
 simulation of the experiment, the amounts adsorbed are 820
 recorded after compression (for adsorption) or after 821
 decompression (for desorption), that is, at times \bar{t}_{2k-1} with k 822
 $= 1, \dots, N_a + N_d$. 823

The second important part of the simulation is to find a 824
 solution of eq 59, where $r(\bar{t})$ is the function shown in Figure 825
 11. It is advantageous for accuracy to find the solution of eq 59 826
 as a succession of solutions, where the different rectilinear parts 827
 of function $r(\bar{t})$ are considered in turn. For each of the $2N_a +$ 828
 $2N_b - 1$ rectilinear parts, one thus defines a time variable, τ_n 829
 and a linear density function, ρ_n of τ_n , as follows 830

$$\tau_n = \frac{\bar{t} - \bar{t}_n}{\bar{t}_{n+1} - \bar{t}_n},$$

$$\rho_n = (1 - \tau_n)\bar{r}_n + \tau_n\bar{r}_{n+1}$$

831 For each rectilinear part, a coverage, $\theta_n(\tau_n)$ is then defined
832 iteratively as the solution of eq 59, rewritten in terms of the
833 new quantities just introduced

$$\frac{d\theta_n}{d\tau_n} = -(\bar{t}_{n+1} - \bar{t}_n)\Delta\tilde{\mu}(\theta_n, \rho_n(\tau_n), \tilde{T}, \tilde{T}_{\Sigma c}, \psi) \quad (23)$$

$$\theta_n(0) = \theta_{n-1}(1) \quad (24)$$

836 This is done for $n = 1, \dots, 2N_a + 2N_d - 1$, where, for $n = 1$,
837 one defines $\theta_1(0) = \theta_{\text{exp},1}$. This last is not an extra assumption
838 because one can replace $\theta_{\text{exp},1}$ by any other value in its vicinity,
839 if one, simultaneously, agrees not to include the first deviation
840 when minimizing the sum of the squared deviations (see item
841 5 in the algorithm below).

842 The final part of the simulation consists of finding the
843 solution of eqs 23 and 24 that best fits the data. It involves the
844 determination of the following set of parameters

$$\{\mathcal{R}, C, C, \tilde{T}_{\Sigma c}, \psi\}$$

845 in a way that minimizes the averaged sum of the squared
846 deviations $(\theta(\bar{t}_{2n-1}) - \theta_{\text{exp},n})^2$. This is done by the following
847 algorithm.

- 848 1 Values are chosen for $\tilde{T}_{\Sigma c}$ and ψ , say 0.3 and 4,
849 respectively.
- 850 2 Using eq 7, the equilibrium isotherm $\theta_e(r_\omega, \tilde{T}_{\text{exp}}, \tilde{T}_{\Sigma c}, \psi)$ is
851 drawn. See the smooth curve in black in the left-hand
852 plot in Figure 12.
- 853 3 The value of C (see eq 21) is calculated, that gives
854 $\theta_e(r_{\text{exp},9}, \tilde{T}_{\text{exp}}, \tilde{T}_{\Sigma c}, \psi) = A_{\text{exp},9}/C$, and the data are replotted
855 with ordinates $\theta_{\text{exp},i} = A_{\text{exp},i}/C$.
- 856 4 Values are chosen for \mathcal{R} and C , say 1 and 0.1, and eqs 23
857 and 24 are solved for all n , as indicated. The value
858 chosen for \mathcal{R} is increased if relaxation, at any
859 experimental point, ends before the equilibrium
860 isotherm is reached (seen graphically as two lines
861 touching, see the left-hand plot of Figure 12.), and the
862 solutions are recalculated. The isotherm is plotted as a
863 blue sawtoothed curve for adsorption, a red sawtoothed
864 curve for desorption: see the left-hand plot on Figure 12.
865 The coverage calculated by the model at the end of each
866 compression is plotted as an asterisk, and the value
867 calculated at the end of each decompression is plotted as
868 a diagonal cross. (Not all asterisks and crosses are shown
869 in the left-hand plot of Figure 12.)
- 870 5 The averaged sum of the squared deviations

$$D2 = \frac{1}{17}$$

$$\left[\sum_{i=2}^9 (\theta^*(r_{\text{exp},i}) - \theta_{\text{exp},i})^2 + \sum_{i=10}^{18} (\theta^\times(r_{\text{exp},i}) - \theta_{\text{exp},i})^2 \right]^{1/2}$$

871 is calculated.

- 872 6 The values of the parameters are those that minimize
873 $D2$.

874 Comments: (i) The value of C determined at the third step
875 above has been taken as the final one with the justification that

the experimental point number 9 is on the flat portion of the 876
isotherm and therefore very close to the equilibrium isotherm. 877
(ii) The value of \mathcal{R} , determined at the fourth step, need not be 878
increased: any larger value will serve the same purpose because 879
reducing the distance to the equilibrium isotherm below a 880
certain small value has no interest. (iii) The value of C turns 881
out to have little influence on the final result: C must be small 882
compared to \mathcal{R} , and small values (0.1, say) give almost 883
horizontal compression or decompression isotherm segments: 884
a smaller value (0.01, say) might be unrealistic (depending on 885
the value of t_i) without noticeably changing the shape of the 886
isotherm segments. 887

The sawtoothed curves of the left-hand plot of Figure 12 are 888
joined at $r_{\text{exp},9}$ as shown by the inset, and can thus be seen as 889
just one isotherm, “anchored” to the experimental points at the 890
last adsorption measurement. 891

The minimum value of $D2$ is 0.00512, and is obtained with 892
 $\mathcal{R} = 0.7$, $C = 0.1$, and

$$\tilde{T}_{\Sigma c} = 0.000,$$

$$\psi = 3.83$$

The right-hand plot of Figure 12 shows theoretical coverage 893
(asterisks and crosses) at pressure values where experimental 894
coverage is given (circles and squares). 895

Comments: (i) The smallness of $\tilde{T}_{\Sigma c}$ indicates that an 896
adsorbate of CO_2 on coal acts like an ideal gas of finite volume 897
molecules. (ii) Model M' , used as described in this section, 898
predicts unique values for $\tilde{T}_{\Sigma c}$ and ψ . In Jessen et al.⁷ (see their 899
Table 2 and Figure 2), adsorption and desorption are assumed 900
to evolve along different equilibrium isotherms, so that two 901
values of ψ result: 3.66 for adsorption and 4.73 for desorption. 902

Turning now to the data reported⁷ concerning the 903
adsorption–desorption at 295.15 K of CH_4 by Wyoming 904
coal, one notes first that, according to the NIST database, the 905
critical temperature for CH_4 is $T_{\text{fc}} = 190.6$ K, so that the 906
ambient CH_4 is supercritical. The adsorbate critical temper- 907
ature being most likely less than the above T_{fc} , the adsorbate is 908
also supercritical. The experiment is then inside the framework 909
of M' because a phase transition for the ambient fluid is 910
excluded, and uniformity of density can be assumed. (See the 911
description of model M' in the Introduction.) The situation is 912
thus similar to that of the CO_2 experiment just gone through, 913
that is, that of a rate-dependent hysteresis isotherm. Following 914
the same procedure, one finds a minimum value of $D2$ equal to 915
0.0067, obtained with $\mathcal{R} = 0.7$, $C = 0.1$, and 916

$$\tilde{T}_{\Sigma c} = 0.3,$$

$$\psi = 5.8$$

Figure 13 shows experimental coverage (circles and squares) 917 f13
and theoretical coverage (asterisks and crosses) calculated at 918
the same pressures. Using data from Table 2,⁷ one finds that 919
the two Langmuir curves that fit the adsorption and desorption 920
 CH_4 curves of Figure 2⁷ yield two values for ψ : 4.61 for 921
adsorption and 8.92 for desorption. 922

5. BACKGROUND MATERIAL

Material given here includes the explicit calculation of the 923
thermodynamic functions of the ambient and adsorbed fluids, 924
that is, pressure and spreading pressure (Section 5.1) and 925
chemical potentials and fugacities (Section 5.2); a subsection 926
devoted to the introduction of Henry's constant (Section 5.3). 927

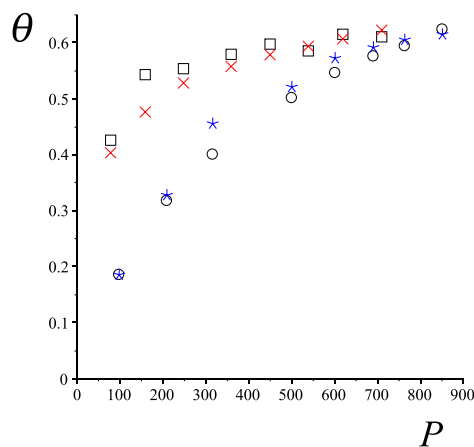


Figure 13. Circles and squares are the experimental data for adsorption (circles) and desorption (squares) of CH₄ by Wyoming coal at 295.15 K.⁷ Blue asterisks (adsorption) and red crosses (desorption) result from model calculations. The horizontal axis gives pressure in PSI. The vertical axis gives dimensionless coverage.

928 A final section (Section 5.4) contains the derivation of the
929 differential equation giving the rate of change of the coverage
930 originating from eq 1.

931 **5.1. Pressure and Spreading Pressure.** As stated in the
932 Introduction, it is assumed that the adsorbed fluid obeys a van
933 der Waals equation of state. The two-dimensional van der
934 Waals equation, used, for example, by Hoory and Prausnitz,¹²
935 is used here

$$936 \quad \Pi = \frac{N_{\Sigma}RT}{\Sigma - N_{\Sigma}\beta} - \frac{\alpha N_{\Sigma}^2}{\Sigma^2} \quad (25)$$

937 What follows is consistent when a monolayer is assumed.
938 The maximum value of N_{Σ} is Σ/β so that the coverage is $N_{\Sigma}\beta/\Sigma$.
939 The particle concentration and coverage are thus

$$940 \quad c_{\Sigma} = N_{\Sigma}/\Sigma \quad (26)$$

$$941 \quad \theta = \beta c_{\Sigma} \quad (27)$$

942 The critical values, identified by a subscript c, are expressed
943 in terms of the constants α and β

$$944 \quad \Pi_c = \frac{\alpha}{27\beta^2}, \quad RT_{\Sigma c} = \frac{8\alpha}{27\beta} \quad (28)$$

945 Concerning the ambient fluid, three equations of state are
946 considered: that of an ideal gas of type 0 (noninteracting zero-
947 volume particles), that of an ideal gas of type 1 (noninteracting
948 nonzero-volume particles), and a plain van der Waals equation

$$949 \quad p^{\text{id}0} = \frac{N_f RT}{V}, \quad p^{\text{id}1} = \frac{N_f RT}{V - N_f b},$$

$$950 \quad p = \frac{N_f RT}{V - N_f b} - \frac{\alpha N_f^2}{V^2} \quad (29)$$

951 Note that, in the type 0 and type 1 cases, one assumes that V
952 is so large that $p^{\text{id}0}$ and $p^{\text{id}1}$ are valid approximations inside
953 some pressure range, but that the van der Waals constants are
954 different from zero, so that it makes sense to speak of critical
955 pressure and temperature.

956 Ambient and adsorbed fluids are assumed to be at the same
957 temperature T . Similar to the two-dimensional case above, one
958 defines

$$c_f = N_f/V \quad (30) \quad 958$$

$$r = bc_f \quad (31) \quad 959$$

The critical values, identified by a subscript c, are expressed
960 in terms of the constants a and b 961

$$P_c = \frac{a}{27b^2}, \quad RT_{fc} = \frac{8a}{27b} \quad (32) \quad 962$$

The critical temperatures of the ambient and adsorbed fluids
963 have different notations because they are known to be
964 different. 965

One now introduces a dimensionless temperature \tilde{T} , a
966 dimensionless spreading pressure $\tilde{\Pi}$, and a dimensionless
967 ambient pressure \tilde{P} , by 968

$$\tilde{T} = \frac{T}{T_{fc}}, \quad \tilde{\Pi} = \frac{\beta\Pi}{RT_{fc}}, \quad \tilde{P} = \frac{bP}{RT_{fc}} = \frac{P}{8P_c} \quad (33) \quad 969$$

Consistently with the definition of \tilde{T} , one defines
970 dimensionless critical temperatures for the ambient and
971 adsorbed fluids 972

$$\tilde{T}_{fc} = 1, \quad \tilde{T}_{\Sigma c} = \frac{T_{\Sigma c}}{T_{fc}} = \frac{\alpha b}{a \beta} \quad (34) \quad 973$$

It follows that 974

$$\tilde{\Pi}(\theta, \tilde{T}, \tilde{T}_{\Sigma c}) = \frac{\tilde{T}\theta}{1 - \theta} - \frac{27}{8} \tilde{T}_{\Sigma c} \theta^2 \quad (35) \quad 975$$

Similarly, the dimensionless versions of eq 29, are 976

$$\tilde{P}^{\text{id}0}(r, \tilde{T}) = \tilde{T}r, \quad \tilde{P}^{\text{id}1}(r, \tilde{T}) = \frac{\tilde{T}r}{1 - r},$$

$$\tilde{P}(r, \tilde{T}) = \frac{\tilde{T}r}{1 - r} - \frac{27}{8} r^2 \quad (36) \quad 977$$

The adsorbed and ambient molecules being chemically
978 identical, α and β are related to a and b . If the gas molecules
979 are spherical and isotropic before and after being adsorbed,
980 then formulas giving α and β in terms of a and b exist¹⁴ and
981 result in $\tilde{T}_{\Sigma c} = 1/2$. Otherwise α and β , and thereby $\tilde{T}_{\Sigma c}$, are
982 often determined by fitting theoretical results to experiments.
983 Some examples of experimentally determined values for $\tilde{T}_{\Sigma c}$ are
984 given in Table 1. It is assumed in the sequel that $\tilde{T}_{\Sigma c} < 1$. 985 t1f14

Table 1. Values of $\tilde{T}_{\Sigma c}$ for the Indicated Adsorbates, on Graphite^a

N ₂	Ar	C ₆ H ₆	CHCl ₃	CFCl ₃
0.36	0.46	0.14	0.39	0.43

^aFrom Hoory and Prausnitz.¹²

Figure 14 defines the symbols used in this article concerning
986 f14 the ambient fluid (left) and the adsorbed fluid (right). In
987 particular, θ_m and θ_M , which often occur, are easily obtainable
988 as solutions of a cubic 989

$$\theta_M^m = \frac{2}{3} \left[1 - \cos \frac{\arccos(2\tau - 1) \pm \pi}{3} \right] \quad (37) \quad 990$$

with 991

$$\tau = \frac{\tilde{T}}{\tilde{T}_{\Sigma c}}. \quad (38) \quad 992$$

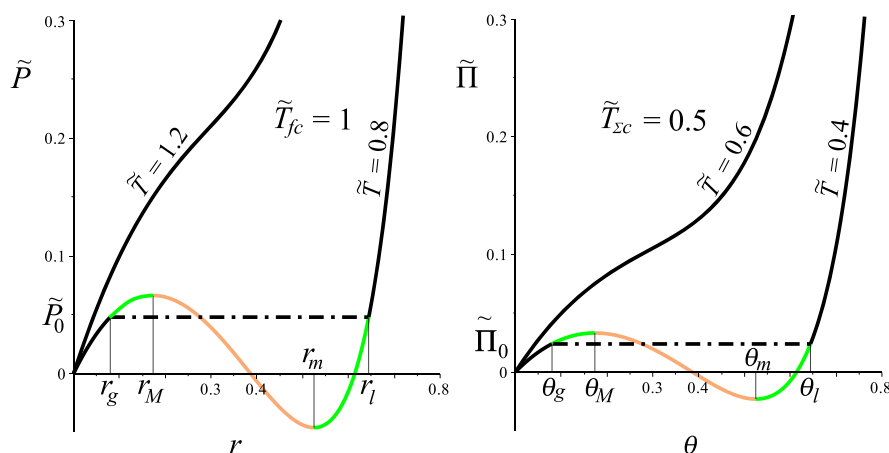


Figure 14. Left: Pressure $\tilde{P}(r, \tilde{T})$, eq 36 (right), for two values of \tilde{T} , one above and one below the critical value, $\tilde{T}_{fc} = 1$, vs r . Right: Spreading pressure $\tilde{\Pi}(\theta, \tilde{T}, 1/2)$, eq 35, for two values of \tilde{T} , one above and one below the critical value $1/2$ vs θ . Concerning the similarity of the curves and also concerning the color and style of lines, see the text at the end of Section 5.1.

993 They are only defined when $\tau \leq 1$, that is, for a subcritical
994 adsorbate. They satisfy $\theta_M \leq \theta_m$ (the equality occurring when τ
995 = 1) and are the abscissas of the intersections of the
996 $\tilde{\Pi}(\theta, \tilde{T}, \tilde{T}_{\Sigma c})$ versus θ curve with its spinodal curve: elsewhere
997 in this article, θ_M and θ_m are referred to as the left and right
998 spinodal coverages.

999 Figure 14 includes the known concepts of physical stability
1000 (black lines), physical metastability (green lines), and physical
1001 instability (orange lines). Equations of state represented by the
1002 black lines joined by the dash-dotted lines are called
1003 reconstructed.¹⁷ A one-phase p-metastable state will eventually
1004 transit, at constant r (or constant θ for the adsorbate), to a
1005 two-phase p-stable state of lower energy on the reconstructed
1006 straight line.

1007 The figure also illustrates the functional relationship implied
1008 by eq 35 and by the third of eq 36, namely: $\tilde{\Pi}(x, \tilde{T}_{\Sigma c}, \tilde{T}_{\Sigma c}) =$
1009 $\tilde{T}_{\Sigma c} \tilde{P}(x, y)$.

1010 **5.2. Chemical Potentials and Fugacities.** The chemical
1011 potentials can now be calculated, up to functions of
1012 temperature. The starting point is

$$dF = -S dT - P dV + \mu_f dN_f$$

1013 One first obtains F by integrating at constant T and N_f one
1014 then obtains μ_f by differentiating F with respect to N_f

$$\mu_f = \lim_{V^* \rightarrow \infty} \left(\left. \frac{\partial F}{\partial N_f} \right|_{T, V^*} + \int_V^{V^*} \left. \frac{\partial P}{\partial N_f} \right|_{T, V'} dV' \right)$$

1015 The limit when $V^* \rightarrow \infty$ of the first term inside the
1016 parenthesis on the right-hand side is the derivative with respect
1017 to N_f of the Helmholtz free energy of the ideal gas.¹⁸ Using its
1018 expression, one gets

$$\mu_f = \lim_{V^* \rightarrow \infty} \left(RT \ln \frac{N_f \mathcal{V}(T)}{V^*} + \int_V^{V^*} \left. \frac{\partial P}{\partial N_f} \right|_{T, V'} dV' \right) \quad (39)$$

1020 where \mathcal{V} has the dimension of molar volume. It can be
1021 obtained by the methods of statistical mechanics,¹⁸ provided
1022 one has specific information about the properties of the
1023 molecules of the ambient fluid,¹⁹ such as moments of inertia
1024 and vibrational frequencies. It is treated here as a function of T ,
1025 referring to Section 5.3 for a further determination that

involves Henry's adsorption constant. Performing the integra- 1026
tion in eq 39, one finds that terms that diverge when $V^* \rightarrow \infty$ 1027
cancel, and one gets 1028

$$\mu_f = RT \ln \frac{\mathcal{V}(T)}{b} + \mu_{f, \text{red}}(r, T) \quad (40) \quad 1029$$

The second term on the right-hand side, here named 1030
reduced chemical potential, has three alternative expressions, 1031
corresponding to the three alternative expressions for the 1032
pressure in eq 29 1033

$$\begin{aligned} \mu_{f, \text{red}}^{\text{id0}}(r, T) &= RT \ln r, \\ \mu_{f, \text{red}}^{\text{id1}}(r, T) &= RT \ln \frac{r}{1-r} + RT \frac{r}{1-r}, \\ \mu_{f, \text{red}}(r, T) &= RT \ln \frac{r}{1-r} + RT \frac{r}{1-r} - \frac{27}{4} RT_{fc} r \end{aligned}$$

The chemical potential of the adsorbed fluid is obtained by a 1034
similar method, μ_{Σ} being then given by a suitably modified 1035
right-hand side of eq 39: V , \mathcal{V} , P , and N_f being changed to A , 1036
 \mathcal{A} , Π , and N_{Σ} . One gets

$$\mu_{\Sigma} = RT \ln \frac{\mathcal{A}(T)}{\beta} + \mu_{\Sigma, \text{red}}(\theta, T) \quad (41) \quad 1037$$

$$\mu_{\Sigma, \text{red}}(\theta, T) = RT \ln \frac{\theta}{1-\theta} + RT \frac{\theta}{1-\theta} - \frac{27}{4} RT_{\Sigma c} \theta \quad (42) \quad 1038$$

The fugacities f_f and f_{Σ} of the ambient and adsorbed fluids 1039
are now introduced, using the definition given by Hoory and 1040
Prausnitz,¹² written below in a form that is equivalent but 1041
slightly different from theirs 1042

$$RT \ln f_f = \lim_{V^* \rightarrow \infty} \left(\int_V^{V^*} \left. \frac{\partial P}{\partial N_f} \right|_{T, V'} dV' + RT \frac{N_f RT}{V^*} \right)$$

A similar formula applies for f_{Σ} where, in the right-hand side 1043
above, V , P , and N_f are changed to A , Π , and N_{Σ} . It is then 1044
easily shown that 1045

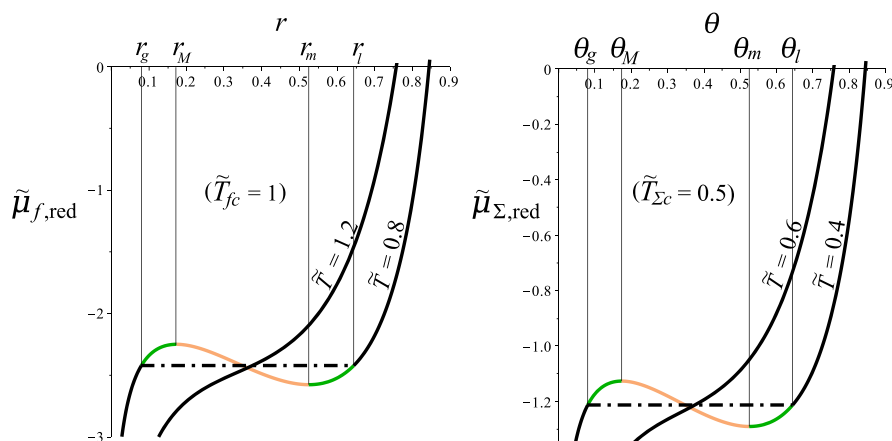


Figure 15. Left: Chemical potential $\tilde{\mu}_{f,\text{red}}(r, \tilde{T})$, eq 49 (left), for two values of \tilde{T} , one above and one below the critical value, $\tilde{T}_{fc} = 1$ vs r . Right: Chemical potential $\tilde{\mu}_{\Sigma,\text{red}}(\theta, \tilde{T}, 1/2)$, eq 46 (left), for two values of \tilde{T} , one above and one below the critical value, $\tilde{T}_{\Sigma c} = 0.5$ vs θ . For both plots, the symbols on the axes and the colors of the lines are as defined in Figure 14. The dash-dotted lines are the reconstructed parts of the chemical potentials, see Figure 14.

$$\mu_f = RT \ln \frac{\mathcal{V}(T)}{b} + RT \ln \frac{bf_f}{RT},$$

$$\mu_{\Sigma} = RT \ln \frac{\mathcal{A}(T)}{\beta} + RT \ln \frac{\beta f_{\Sigma}}{RT}$$

1046 Comparing these equations with 40 and 41, one obtains

$$\mu_{f,\text{red}} = RT \ln \frac{bf_f}{RT}, \quad \mu_{\Sigma,\text{red}} = RT \ln \frac{\beta f_{\Sigma}}{RT} \quad (43)$$

1048 It is possible to show that one gets the expected result that Π
1049 and f_{Σ} become equal at the vanishing spreading pressure:
1050 according to eqs 26 and 27, $\Sigma = \beta N_{\Sigma}/\theta$ and letting $\Sigma \rightarrow \infty$ in
1051 eq 25, one gets $\Pi \approx RT\theta/\beta$. On the other hand, when $\theta \rightarrow 0$,
1052 then eq 42 shows that $\mu_{\Sigma,\text{red}} \approx RT \ln \theta$ which, combined with
1053 eq 43, gives $f_{\Sigma} \approx RT\theta/\beta \approx \Pi$. It is similarly easy to show that P
1054 $\approx f_f$ when $V \rightarrow \infty$.

1055 It is convenient to introduce dimensionless chemical
1056 potentials and dimensionless fugacities to accompany the
1057 dimensionless pressures introduced in Section 5.1. The
1058 definitions are suggested by eqs 40–42 for the chemical
1059 potentials and by eq 43 for the fugacities

$$\begin{aligned} \tilde{\mu}_{\Sigma,\text{red}} &= \frac{\mu_{\Sigma,\text{red}}}{RT_{fc}}, & \tilde{\mu}_{f,\text{red}} &= \frac{\mu_{f,\text{red}}}{RT_{fc}}, \\ \tilde{f}_{\Sigma} &= \frac{\beta f_{\Sigma}}{RT_{fc}}, & \tilde{f}_f &= \frac{bf_f}{RT_{fc}} \end{aligned} \quad (44)$$

1061 Equation 43 becomes

$$\frac{\tilde{f}_{\Sigma}}{\tilde{T}} = \exp \frac{\tilde{\mu}_{\Sigma,\text{red}}}{\tilde{T}}, \quad \frac{\tilde{f}_f}{\tilde{T}} = \exp \frac{\tilde{\mu}_{f,\text{red}}}{\tilde{T}} \quad (45)$$

1063 One obtains, for the adsorbed fluid,

$$\begin{aligned} \tilde{\mu}_{\Sigma,\text{red}}(\theta, \tilde{T}, \tilde{T}_{\Sigma c}) &= \tilde{T} \ln \frac{\theta}{1-\theta} + \tilde{T} \frac{\theta}{1-\theta} - \frac{27}{4} \tilde{T}_{\Sigma c} \theta, \\ \tilde{f}_{\Sigma}(\theta, \tilde{T}, \tau) &= \frac{\tilde{T} \theta}{1-\theta} \exp \left(\frac{\theta}{1-\theta} - \frac{27\theta}{4\tau} \right) \end{aligned} \quad (46)$$

1065 Similar expressions for the ambient fluid follow, where the
1066 particular cases of an ideal gas of type 0 or 1 are included:

$$\tilde{\mu}_{f,\text{red}}^{\text{id0}}(r, \tilde{T}) = \tilde{T} \ln r, \quad \tilde{f}_f^{\text{id0}}(r, \tilde{T}) = \tilde{T}r \quad (47) \quad 1067$$

$$\begin{aligned} \tilde{\mu}_{f,\text{red}}^{\text{id1}}(r, \tilde{T}) &= \tilde{T} \ln \frac{r}{1-r} + \tilde{T} \frac{r}{1-r}, \\ \tilde{f}_f^{\text{id1}}(r, \tilde{T}) &= \frac{\tilde{T}r}{1-r} \exp \frac{r}{1-r} \end{aligned} \quad (48) \quad 1068$$

$$\begin{aligned} \tilde{\mu}_{f,\text{red}}(r, \tilde{T}) &= \tilde{T} \ln \frac{r}{1-r} + \tilde{T} \frac{r}{1-r} - \frac{27}{4}r, \\ \tilde{f}_f(r, \tilde{T}) &= \frac{\tilde{T}r}{1-r} \exp \left(\frac{r}{1-r} - \frac{27r}{4\tilde{T}} \right) \end{aligned} \quad (49) \quad 1069$$

1070 Functions 46 and 49 are shown in Figure 15. 1070 f15

1071 The following remarks refer to Figures 14 and 15. 1071

- 1072 Comparing eq 46 and the van der Waals version in eq
1073 49, one sees that $\tilde{T}_{\Sigma c} \tilde{\mu}_{f,\text{red}}(x, y) = \tilde{\mu}_{\Sigma,\text{red}}(x, \tilde{T}_{\Sigma c} y, \tilde{T}_{\Sigma c})$ and
1074 Figure 15 illustrates this equality for $\tilde{T}_{\Sigma c} = 1/2$. 1074
- 1075 Figures 14 and 15 illustrate the following easily provable
1076 equalities: 1076

$$\theta \frac{\partial}{\partial \theta} \tilde{\mu}_{\Sigma,\text{red}} = \frac{\partial}{\partial \theta} \tilde{\Pi}, \quad r \frac{\partial}{\partial r} \tilde{\mu}_{f,\text{red}} = \frac{\partial}{\partial r} \tilde{P}$$

1077 These show that the chemical potentials and the pressures,
1078 when plotted against their first argument, have local extrema at
1079 the same values of that argument. Also, the chemical potentials
1080 can be reconstructed by localizing the points with abscissas r_g
1081 and r_l (alternatively θ_g and θ_l), then replacing the loop between
1082 them by the horizontal straight line segment joining them. See
1083 Figure 15 where the lines have been drawn in the manner of
1084 Figure 14, with the same meanings. 1084

1085 It is assumed that the ambient fluid is constrained to always
1086 be in the same phase. There are no constraints on the adsorbed
1087 fluid, however, so that it can undergo a phase transition. 1087

1088 **5.3. Henry's Adsorption Constant.** Using eqs 40 and 41,
1089 an expression for the $\Delta\mu$ of eq 2 can now be written as 1089

$$\Delta\mu/L = -RT \ln \left(\frac{\beta \mathcal{V}(T)}{b \mathcal{A}(T)} \right) - \mu_{f,\text{red}} + \mu_{\Sigma,\text{red}} \quad (50) \quad 1090$$

1091 The unknown function of T on the right-hand side is found
1092 by using the method used by Hoory and Prausnitz.¹² Using eq
1093 43, eq 50 can be written as 1093

$$\Delta\mu/L = -RT \ln\left(\frac{\beta \mathcal{V}(T)}{b \mathcal{A}(T)}\right) - RT \ln\left(\frac{b f_f}{\beta c_\Sigma}\right)$$

This formula remains valid when ambient gas and adsorbate are at equilibrium with each other at very low pressure: then, $\Delta\mu = 0$ and, according to the paragraph following eq 43, $f_\Sigma = \Pi = RTc_\Sigma$ and $f_f = P = RTc_f$. As the function of T does not depend on the physical situation, one obtains

$$RT \ln\left(\frac{\beta \mathcal{V}(T)}{b \mathcal{A}(T)}\right) = -RT \ln\left(\frac{b c_f}{\beta c_\Sigma}\right) \quad (51)$$

The pressure being low, the concentrations are small and c_Σ/c_f is Henry's adsorption constant, K_H . It is actually a function of temperature and of molecular properties, as defined in the literature that is used in this article.²⁰ It is convenient to introduce a dimensionless Henry constant, \tilde{K}_H , and the following expressions define the notation:

$$c_\Sigma = K_H c_f, \quad \tilde{K}_H = \beta K_H / b \quad (52)$$

Then eq 51 gives

$$\frac{\beta \mathcal{V}(T)}{b \mathcal{A}(T)} = \tilde{K}_H(\tilde{T}, \mathcal{D}) \quad (53)$$

where \mathcal{D} is a set of constants that determine the interaction between adsorbent and adsorbate, and thereby the sorption properties.²⁰ Note that, with the notation introduced in eqs 31 and 27,

$$\theta = \tilde{K}_H r \quad (54)$$

when the pressure goes to zero.

Using eq 53 in eq 50 one obtains an expression for $\Delta\mu$ where the unknown function of temperature is replaced by Henry's "constant"

$$\Delta\mu/L = -RT \ln \tilde{K}_H(\tilde{T}, \mathcal{D}) - \mu_{f,\text{red}} + \mu_{\Sigma,\text{red}}$$

Introducing dimensionless chemical potentials by using the two first equations in the set 44, one obtains

$$\Delta\tilde{\mu} = \Delta\mu/(LRT_{fc}) \quad (55)$$

$$= \tilde{\mu}_{\Sigma,\text{red}}(\theta, \tilde{T}, \tilde{T}_{\Sigma c}) - \tilde{\mu}_{f,\text{red}}(r, \tilde{T}) - \psi(\tilde{T}, \mathcal{D}) \quad (56)$$

where

$$\psi = \tilde{T} \ln \tilde{K}_H(\tilde{T}, \mathcal{D}) \quad (57)$$

The dependence of ψ on a number of constants gathered in the set \mathcal{D} implies that ψ can be seen as an experimental quantity that determines, at a given temperature, the adsorption properties of the combination of the fluid and adsorbing surface. See Section 4.

Experimental and theoretical results are cited below so as to establish an order of magnitude for the interval in which values of ψ are found.

K_H is usually written as $K_H = A_0 \exp(T_0/T)$, where RT_0 is called the adsorption potential,¹⁴ and A_0 is a function of T . An explicit expression for $A_0(T)$, in terms of a set of constants, is given in the framework of a model described by Dolgonosov.²⁰ The set \mathcal{D} of constants is given by Dolgonosov²⁰ for 40 adsorbate molecules on a graphite adsorbent, and curves of K_H versus T are shown, together with experimental values, for selected temperature intervals. A selection of seven such curves is shown in Figure 16 (thin solid lines), covering a wide range

of ψ -values. In addition, the five curves drawn with thick solid lines originate from data given in Ross and Olivier,¹⁴ Finally, the broken line curve originates from data given by Saha et al.,²¹ and the long thick solid line is the plot of Ψ_u defined by eq 8.

Figure 16 indicates that for temperatures and for adsorbate/adsorbent pairs that are industrially interesting, ψ is an

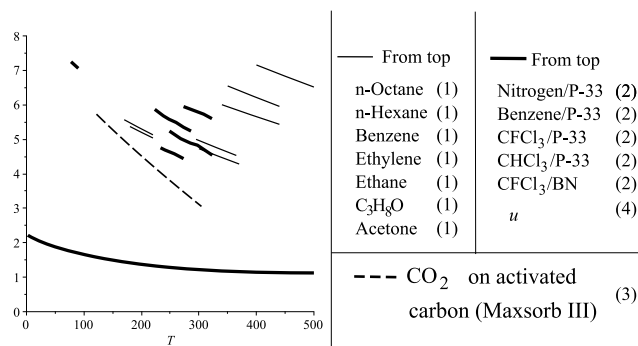


Figure 16. ψ vs T , from the sources indicated by the numbers in parentheses. (1) are from Dolgonosov;²⁰ (2) from Ross and Olivier,¹⁴ where P-33 refers to graphitized carbon and BN to boron nitride; (3) from Saha et al.;²¹ and (4) is eq 8.

approximately linear, slowly decreasing function of temperature, with numerical values roughly inside the interval 3 to 8. Values lower than 3 probably exist but characterize industrially uninteresting low adsorbents.

5.4. Differential Equation for the Coverage. A differential equation for the coverage θ is here written by using eq 27 on the left-hand side of eq 1, eq 55 on its right-hand side, and then by introducing dimensionless time, \tilde{t} , by

$$\tilde{t} = \frac{t}{t_r}, \quad \text{where } t_r = \frac{1}{L\beta RT_{fc}} \quad (58)$$

One obtains

$$\dot{\theta} = -\Delta\tilde{\mu}(\theta, r, \tilde{T}, \tilde{T}_{\Sigma c}, \psi) \quad (59)$$

where the dot on the left-hand side now denotes derivation with respect to \tilde{t} . In $\Delta\tilde{\mu}$ (see eq 56), $\tilde{\mu}_{f,\text{red}}$ is one of the three alternative equations given on the left-hand column of the set 47 to 49. The medium being homogeneous, and density being uniform, there is no space dependence, and eq 59 is to be solved in time, with an initial condition giving θ at time zero. The solution is sought for $\tilde{t} > 0$, and the coverage θ is in the interval (0, 1).

Most of this article is concerned with the equilibrium and the nonequilibrium solutions of eq 59, with the aim of determining their general characteristics. One is thus led to look at the solutions for different values of the parameters, so that it is important to know the intervals in which, in particular, t_r , $\tilde{T}_{\Sigma c}$, and ψ are likely to be in actual applications. Concerning $\tilde{T}_{\Sigma c}$ and ψ , see Sections 5.1 and 5.3, respectively.

Reference time t_r is unknown because of its dependence on L , a constant that, by definition, must be determined by dedicated experiments. As time-dependent results presented in this article are expressed in terms of dimensionless time, it is useful to have an order of magnitude for t_r . According to an article by Gleysteen and Deitz²² published in 1945 on the sorption of nitrogen on carbon adsorbents, steady state is attained in about 20 min, meaning that sorption does not

1182 measurably change for larger time values. More recently
 1183 (1984), in Ruthven's book on adsorption,^{23,24} sorption
 1184 experiments of ethane on Linde 4A zeolite are cited, showing
 1185 about the same time to steady state. Somewhat more extensive
 1186 measurements were reported in 2010 by Battistutta et al.⁸ on
 1187 the sorption of methane, nitrogen, and carbon dioxide on dry
 1188 coal. These showed that, to measure an equilibrium isotherm,
 1189 the waiting time between pressure changes can vary between a
 1190 day and 10 days, depending on the gas adsorbed and on
 1191 temperature. It thus seems that values of t_i should be expected
 1192 to be anything between a half hour and a week.

1193 ■ AUTHOR INFORMATION

1194 Corresponding Author

1195 *E-mail: paul.papatzacos@uis.no.

1196 ORCID

1197 Paul Papatzacos: 0000-0002-5193-4597

1198 Notes

1199 The author declares no competing financial interest.

1200 ■ ACKNOWLEDGMENTS

1201 The author thanks Professor Aksel Hiorth for a number of
 1202 clarifying discussions.

1203 ■ NOMENCLATURE

1204 Latin Symbols

1205 A , $A_{\text{exp},i}$ coverage in SCF per ton, coverage of experimental
 1206 point i on a graph in SCF per ton. See Section 4; \mathcal{A} , function
 1207 of temperature and of molecular properties such as vibrational
 1208 frequencies. It has the dimension of area per mole. See eq 41;
 1209 a , b , van der Waals constants. See eq 29; c_{Σ} , c_{β} number of
 1210 adsorbed molecules per unit area (see eq 26), number of
 1211 ambient molecules per unit volume (see eq 30); C , constant of
 1212 dimension SCF per ton. See eq 21; C , in an adsorption
 1213 experiment, estimated time used to compress the ambient gas
 1214 from the lowest to the highest pressure, at a constant rate. See
 1215 eq 22; \mathcal{D} , set of constants determining the interaction between
 1216 adsorbate and adsorbent. See eq 53 and the statement
 1217 following it; E_{m} , E_{M} functions of τ introduced to define the
 1218 vertical boundaries of the hysteresis loop. See eq 18; f_{Σ} , f_{β}
 1219 fugacities of the adsorbate and of ambient fluid. See Section
 1220 5.2; \tilde{f}_{Σ} , \tilde{f}_{β} dimensionless fugacities of the adsorbate and
 1221 ambient fluids. Defined in eq 44; $\tilde{f}_i^{\text{id}0}$, $\tilde{f}_i^{\text{id}1}$, dimensionless
 1222 fugacities of the ideal ambient fluid with zero volume particles
 1223 (superscript 0), or nonzero volume particles (superscript 1).
 1224 See eq 47 (right) and 48 (right); F , Helmholtz free energy. See
 1225 Section 5.2; K_{H} , \tilde{K}_{H} dimensional and dimensionless Henry
 1226 constant of adsorption. See eq 52; L , phenomenological
 1227 constant. See eq 2; N_{Σ} , N_{β} number of adsorbed moles on Σ
 1228 (see eq 25), number of ambient moles in V (see eq 29); $P^{\text{id}0}$,
 1229 $P^{\text{id}1}$, P , ambient fluid pressure for ideal fluid with zero volume
 1230 molecules (superscript 0), with nonzero volume molecules
 1231 (superscript 1), and for a van der Waals fluid. See eq 29; P_{c}
 1232 ambient fluid critical pressure. See eq 32 (left); $P_{\text{exp},i}$ $\tilde{P}_{\text{exp},i}$
 1233 pressure (PSI, dimensionless) of experimental point i . See
 1234 Figure 10; $\tilde{P}^{\text{id}0}$, $\tilde{P}^{\text{id}1}$, \tilde{P} , dimensionless versions of $P^{\text{id}0}$, $P^{\text{id}1}$, P .
 1235 See eq 33 (right); \tilde{P}_0 , dimensionless saturation pressure. See
 1236 Figure 14 (left); r , ratio of number of ambient molecules per
 1237 unit volume to its maximum value. See eqs 30 and 31; r_{e}
 1238 equilibrium value of r , at a given ambient temperature and
 1239 pressure; r_{g} , r_{v} , r -values for the saturated gas and saturated
 1240 liquid, obtained through the Maxwell construction. See Figure

14; r_{v} , r_1 , r_2 , r -values locating the center of the hysteresis loop,
 its left- (subscript 1) and right-hand (subscript 2) vertical
 boundaries. See eqs 10 and 17; r_{m} , r_{M} , r -values of the local
 minimum or local maximum, of a van der Waals ambient fluid.
 See Figure 14 (left); r_{c} , r_{v} parameters characterizing a
 compression-decompression cycle. See Figure 7; $r_{\text{exp},i}$ r -value
 of experimental point number, i , such that $P(r_{\text{exp},i}, T_{\text{exp}}) = P_{\text{exp},i}$.
 See Section 4 and Figure 10; \bar{r}_{v} array of r -values. See Section 4,
 following eq 22; R , gas constant; S , entropy. See Section 5.2; t ,
 \tilde{t} , t_{v} time, dimensionless time, reference time. See eq 58; \tilde{t}_{d} ,
 cycle duration, in a compression–decompression cycle. See
 Figure 7; \bar{t}_{v} array of t -values. See Section 4, following eq 22; T ,
 \tilde{T} , dimensional, dimensionless temperature. See eq 33; T_{exp} ,
 \tilde{T}_{exp} temperature at which a sorption measurement is carried
 out, its dimensionless counterpart; $T_{\Sigma_{\text{c}}}$, T_{ic} , $\tilde{T}_{\Sigma_{\text{c}}}$, \tilde{T}_{ic} critical
 temperature of adsorbate fluid, of ambient fluid, and their
 dimensionless counterparts; ν , rate of compression. See eq 22;
 V , volume variable in a three dimensional equation of state. See
 eq 29; \mathcal{V} , function of temperature and of molecular properties
 such as vibrational frequencies. It has the dimension of volume
 per mole. See eq 39

1262 Greek Symbols

1263 α , β , van der Waals constants. See eq 25; $\Delta\mu$, $\Delta\tilde{\mu}$, see eqs 1, 2,
 59, and 56; θ , ratio of number of adsorbed molecules per unit
 area to its maximum value (coverage). See eq 27; θ_{e} ,
 equilibrium value of θ , at a given ambient temperature and
 pressure; θ_{m} , θ_{M} θ -values of the local minimum, or local
 maximum, of a van der Waals adsorbed fluid. See Figure 14
 (right), and eq 37. θ_{M} and θ_{m} are also referred to as the left and
 right spinodal coverages; θ_{ea} , θ_{ed} values of equilibrium
 coverage for a subcritical adsorbate. Subscript ea indicates
 the adsorption value, subscript ed indicates the desorption
 value. See eqs 11 and 12; μ_{Σ} , μ_{β} chemical potential of the
 adsorbate and of ambient fluid. See Section 5.2; $\mu_{\text{f,red}}^{\text{id}0}$, $\mu_{\text{f,red}}^{\text{id}1}$,
 $\mu_{\text{f,red}}$ reduced chemical potential of the ideal ambient fluid with
 zero volume molecules (superscript 0), with nonzero volume
 molecules (superscript 1), and for a van der Waals fluid. See
 the three equations following eq 40; $\mu_{\Sigma,\text{red}}$ reduced chemical
 potential of the adsorbate. See eq 42; $\tilde{\mu}_{\Sigma,\text{red}}$ dimensionless
 reduced chemical potential of the adsorbate. See eq 46 (left);
 $\tilde{\mu}_{\text{f,red}}^{\text{id}0}$, $\tilde{\mu}_{\text{f,red}}^{\text{id}1}$, $\tilde{\mu}_{\text{f,red}}$ dimensionless reduced chemical potential of
 the ambient fluid for three cases: ideal fluid with zero volume
 molecules (superscript id 0), ideal fluid with nonzero volume
 molecules (superscript id 1), and van der Waals. See eqs 47–
 49 (left); Π , $\tilde{\Pi}$, spreading pressure of the adsorbate,
 dimensional (eq 25) and dimensionless (eq 35); $\tilde{\Pi}_0$,
 dimensionless saturation spreading pressure. See Figure 14
 (right); Π_{c} adsorbate critical pressure. See eq 28 (left); Σ , area
 variable in a two-dimensional equation of state. See eq 25; τ ,
 see eq 38; ψ , function of temperature and of the set \mathcal{D} . Related
 to the Henry constant by eq 57; Ψ_{w} , Ψ_{m} , Ψ_{M} functions of \tilde{T}
 and $\tilde{T}_{\Sigma_{\text{c}}}$, defined by eqs 8, 13, and 14. See also Figures 3 and 5

1293 ■ ADDITIONAL NOTES

1294 ^aMAPLE's implicitplot has been used.

1295 ^bMaple has been used, and the method of solution is rfk45,
 1296 described as "Fehlberg fourth–fifth order Runge–Kutta".

1297 ■ REFERENCES

1298 (1) Morishige, K.; Shikimi, M. Adsorption hysteresis and pore
 1299 critical temperature in a single cylindrical pore. *J. Chem. Phys.* **1998**,
 1300 *108*, 7821–7824.

- 1301 (2) Hill, T. L. Statistical Mechanics of Multimolecular Adsorption.
1302 III. Introductory Treatment of Horizontal Interactions. Capillary
1303 Condensation and Hysteresis. *J. Chem. Phys.* **1947**, *15*, 767–777.
- 1304 (3) Papatzacos, P.; Skjæveland, S. M. Relative Permeability From
1305 Thermodynamics. *SPE J.* **2004**, *9*, 47–56.
- 1306 (4) Alfé, D.; Gillan, M. J. *Ab initio* statistical mechanics of surface
1307 adsorption and desorption. I. H₂O on MgO (001) at low coverage. *J.*
1308 *Chem. Phys.* **2007**, *127*, 114709.
- 1309 (5) Ball, P. C.; Evans, R. On the Mechanism for Hysteresis of Gas
1310 Adsorption on Mesoporous Substrates. *Europhys. Lett.* **1987**, *4*, 715–
1311 721.
- 1312 (6) Zhao, H.; Lai, Z.; Firoozabadi, A. Sorption Hysteresis of Light
1313 Hydrocarbons and Carbon Dioxide in Shale and Kerogen. *Sci. Rep.*
1314 **2017**, *7*, 16209.
- 1315 (7) Jessen, K.; Tang, G.-Q.; Kovscek, A. R. Laboratory and
1316 Simulation Investigation of Enhanced Coalbed Methane Recovery
1317 by Gas Injection. *Transp. Porous Media* **2008**, *73*, 141–159.
- 1318 (8) Battistutta, E.; van Hemert, P.; Lutynski, M.; Bruining, H.; Wolf,
1319 K.-H. Swelling and sorption experiments on methane, nitrogen and
1320 carbone dioxide on dry Selar Cornish coal. *Int. J. Coal Geol.* **2010**, *84*,
1321 39–48.
- 1322 (9) Wang, K.; Wang, G.; Ren, T.; Cheng, Y. Methane and Carbon
1323 Dioxide sorption hysteresis on coal: A critical review. *Int. J. Coal Geol.*
1324 **2014**, *132*, 60–80.
- 1325 (10) Papatzacos, P. Macroscopic Two-phase Flow in Porous Media
1326 Assuming the Diffuse-interface Model at Pore Level. *Transp. Porous*
1327 *Media* **2002**, *49*, 139–174.
- 1328 (11) Myers, A. L.; Prausnitz, J. M. Thermodynamics of Mixed-Gas
1329 Adsorption. *AIChE J.* **1965**, *11*, 121–127.
- 1330 (12) Hoory, S. E.; Prausnitz, J. M. Monolayer adsorption of gas
1331 mixtures on homogeneous and heterogeneous solids. *Chem. Eng. Sci.*
1332 **1967**, *22*, 1025–1033.
- 1333 (13) Arrowsmith, D. K.; Pace, C. M. *Ordinary Differential Equations*;
1334 Chapman and Hall, 1982.
- 1335 (14) Ross, J. P.; Olivier, S. *On Physical Adsorption*; Interscience
1336 Publishers, 1964.
- 1337 (15) Olver, F. W. J.; Lozier, D. W.; Boisvert, R. F.; Clark, C. W.
1338 *NIST Handbook of Mathematical Functions*; National Institute of
1339 Standards and Technology and Cambridge University Press, 2010.
- 1340 (16) Ang, W. T.; Garmón, F. A.; Khosla, P. K.; Riviere, C. N.
1341 Modeling Rate-Dependent Hysteresis in Piezo-Electric Actuators.
1342 *Proceedings of the 2003 IEEE/RSJ International Conference on Intelligent*
1343 *Robots and Systems*, 2003.
- 1344 (17) Rowlinson, J. S.; Widom, B. *Molecular Theory of Capillarity*;
1345 Oxford University Press, 1982.
- 1346 (18) Hill, T. L. *An Introduction to Statistical Thermodynamics*; Dover
1347 Publications, 1986.
- 1348 (19) Papatzacos, P. The Helmholtz free energy of pure fluid
1349 substances and fluid mixtures. *Proceedings of the 8th International*
1350 *Conference on Heat Transfer, Fluid Mechanics and Thermodynamics*,
1351 2011; pp 845–852.
- 1352 (20) Dolgonosov, A. M. Calculation of Adsorption Energy and
1353 Henry Law Constant for Nonpolar Molecules on a Nonpolar Uniform
1354 Adsorbent. *J. Phys. Chem. B* **1998**, *102*, 4715–4730.
- 1355 (21) Saha, B. B.; Jribi, S.; Koyama, S.; El-Sharkawy, I. I. Carbon
1356 Dioxide Adsorption Isotherms on Activated Carbons. *J. Chem. Eng.*
1357 *Data* **2011**, *56*, 1974–1981.
- 1358 (22) Gleysteen, L. F.; Deitz, V. R. Hysteresis in the physical
1359 adsorption of nitrogen on bone char and other adsorbents. *J. Res. Natl.*
1360 *Bur. Stand.* **1945**, *35*, 285–307.
- 1361 (23) Ruthven, D. M. *Principles of Adsorption and Adsorption*
1362 *Processes*; Wiley-Interscience Publications, 1984.
- 1363 (24) Reference 23, Figure 6.5.